A NOVEL APPROACH TO CHARACTERIZE THE MEMBRANE- DISRUPTING ACTIVITY OF ANTIMICROBIAL PEPTIDES USING ^{2}H SOLID-STATE NMR OF WHOLE ESCHERICHIA COLI

JAMES PIUS

A Novel Approach to Characterize the Membrane-disrupting Activity of Antimicrobial Peptides using ^{2}H Solid-State NMR of Whole *Escherichia coli*

July 10th, 2012, Memorial University of Newfoundland

Submitted in partial fulfillment of the requirements for the degree Master of Science

Department of Biochemistry

Memorial University of Newfoundland

St. John's, NL, A1B 3X9

2012

Abstract

Antimicrobial peptides (AMPs) are ubiquitous molecules that can display antimicrobial activity against bacteria, viruses, protozoa and various other pathogens. They are commonly short, cationic amphipathic peptides that may offer valuable bases for the development of new therapeutic agents. AMPs can have diverse mechanisms of antibacterial activity; all these mechanisms involve interacting with the bacterial membrane to some degree. In order to better understand these mechanisms, a variety of biophysical techniques including solid-state NMR (SSNMR) have been used to study AMPs in model lipid systems. However, these simple model systems do not reflect the complexity of whole cells with which AMPs interact *in vivo*. In order to bridge the gap between SSNMR studies of AMPs in model membranes and the true biological context of AMPs, a procedure was developed which incorporates high levels of ^{2}H NMR labels specifically into the cell membrane of *Escherichia coli*. Using these labeled cells, ^{2}H NMR spectra were acquired both in the absence and presence of the AMP MSI-78. The effects of MSI-78 on bacterial membrane disorder were quantified in terms of the first moment of the spectrum, which directly reflects the activity of MSI-78 in disrupting the membranes of whole bacteria. Data obtained from NMR measurements show an increased disorder in the orientation of lipids in the cell with increasing levels of MSI-78. These effects are observed at molar peptide:lipid (P:L) ratios 30 times greater than that used for model lipid systems and 25 times less than the ratios needed to inhibit cell growth. Based on the observed results, MSI-78 can disrupt the lipid order in the cell envelope even at sublethal concentrations.

Acknowledgements

I would like to take this opportunity to acknowledge those who have helped me complete this project. First and foremost, I would like to thank my supervisors, Dr. Valerie Booth and Dr. Mike Morrow for their support, encouragement and advice, which have been very valuable both professionally and personally. I am grateful to Dr. Matthew Rise for his support as a member of the advisory committee. I would also like to thank Dr. Andrew Lang for use of his laboratory equipment and his expertise on several microbiological techniques. I am also thankful to other members of our research group, Ms. Donna Jackman, Mr. Dharamaraju Palleboina, Dr. Mark McDonald, Mr. Nathan Agnew, Dr. Michael Hayley, Mr. Mitchell Browne and Dr. Muzaddid Sarker, whose cooperation was indispensable and their friendship immensely appreciated. Finally, I would like to thank the Research and Development Corporation of Newfoundland and Labrador (RDC) and the Natural Sciences and Engineering Research Council of Canada (NSERC) for their financial support throughout this project.

Note: A major portion of this research has been published in a Biochemistry paper entitled "^{2}H Solid-State Nuclear Magnetic Resonance Investigation of Whole *Escherichia coli* Interacting with Antimicrobial Peptide MSI-78 [Pius et al., 2012 (Biochemistry. 2012 Jan 10; 51 (1): 118-25. Epub 2011 Dec 7.), DOI: 10.1021/bi201569t]." I performed the work presented in this thesis with the exception of the peptide synthesis, which was accomplished with help from Donna Jackman (Booth lab, Biochemistry, MUN). This is a true copy of the thesis, including any required final revisions, as accepted by my supervisors, supervisory committee member and examiners.

Table of Contents

List of Figures

List of Tables

List of Abbreviations

Δ_2	mean square width of the distribution of splittings
ACC	acetyl-CoA carboxylase
AMPs	antimicrobial peptides
CL	cardiolipin
CGSC	Coli Genetic Stock Center
CFUs	colony forming units
DSC	differential scanning calorimetry
DMF	dimethylformamide
E coli	*Escherichia coli*
Fmoc	O-fluorenylmethyloxycarbonyl
GaP	genomics and proteomics
HPLC	high-pressure liquid chromatography
HoBt	1-hydroxy-benzotriazole
kan	kanamycin resistance gene
LPS	lipopolysaccharides
LB	Luria-Bertani
MTT	3-(4,5-dimethylthiazol-2-yl)-diphenyl tetrazolium bromide
MALDI-TOF	matrix-assisted laser desorption/ionization-time of flight mass spectrometry
MRSA	methicillin-resistant *Staphylococcus aureus*

mAU	milli-absorbance units
MIC	minimal inhibitory concentration
MD	molecular dynamics
M_1	first moment
M_2	second moment
NSERC	National Sciences and Engineering Research Council of Canada
NMR	nuclear magnetic resonance
OCD	oriented circular dichroism
POPC	1-palmitoyl-2-oleoyl-sn-glycerol-3-phosphocholine
POPE	1-palmitoyl-2-oleoyl-sn-glycerol-3-phosphoethanolamine
POPG	1-palmitoyl-2-oleoyl-sn-glycero-3-phosphoglycerol
P : L	peptide : lipid
PE	phosphatidylethanolamine
PG	phosphatidylglycerol
RDC	Research and Development Corporation of Newfoundland & Labrador
SSNMR	solid-state nuclear magnetic resonance
TFA	trifluroacetic acid
VBNC	viable but not culturable
w/w	peptide / dry cell weight

1. Introduction

The ever-increasing resistance of pathogens against commonly used antibiotics is a growing health concern [1]. At present, over sixty percent of infections by *Staphylococcus aureus* – the most commonly acquired hospital infection – are resistant to various conventional small molecule drugs. Some strains even show a resistance to vancomycin, an antibiotic often used as a last resort when others have failed [2]. Currently in US hospitals, more people die of infections by *Staphylococcus aureus* than HIV/AIDS and tuberculosis combined [3]. There have also been reports of the emergence of highly resistant Gram-negative bacteria *(Escherichia coli* and *Pseudomonas aeruginosa* in particular) with some appearing to be pan-resistant (resistant to all known antibiotics) [4]. As a consequence of this emerging resistance, physicians are forced to rely on antiquated drugs such as colistin, which was previously abandoned for antibiotic use due to its significant toxicity [5]. This increasing resistance poses a grave threat in particular to immunocompromised individuals – elderly, patients undergoing surgery, neonates, etc. – and as such there is an urgent need for new and effective antimicrobial agents [6].

Demand for the development of new antibiotics has led to a significant interest in antimicrobial peptides (AMPs) [7], [8], [9]. AMPs have been discovered in a variety of microorganisms, plant, invertebrate and vertebrate species, including humans [9]. Organisms with no or underdeveloped adaptive immunity (e.g. insects [10]) rely particularly on their innate immune system, of which AMPs are an integral part [9].

AMPs are evolutionarily conserved and have been protecting organisms from bacterial pathogens for millions of years, suggesting that bacteria cannot easily develop resistance against them [7]. This makes AMPs an attractive novel class of antibiotics, since they hold the promise of rectifying the current threat of antibiotic resistance.

Despite the identification of thousands of natural AMPs and the possibility of engineering many synthetic variants, very few have proceeded to clinical trials, and even fewer have shown success as therapeutic agents [7]. The U.S Food and Drug Administration has approved only a few AMPs as anti-infective drugs [11]. Although active in vitro, AMPs are only effective in animal models of infection at very high doses. This is close to the toxic levels for the host cell and does not justify their use given the risk [11]. Thus, in order to use AMPs as therapeutic agents, they need to be modified to make them more active and simultaneously more selective for pathogens. The solution to this obstacle may lie in better understanding of the biological and physiochemical properties of AMPs.

Although it would be almost a century before the molecular agents would be identified, investigation of AMPs began in the late 1870s through two independent fields of research: studies on mechanisms used by mammalian granulocytes to kill bacteria, and mechanisms used by other organisms to kill bacteria [12]. At the time, the precise identities of the AMPs involved were not clearly understood. Two decades later, around the time of Alexander Fleming's discovery of penicillin, antimicrobial agents (including AMPs) were classified based on their predisposition for either Gram-negative

or Gram-positive bacteria [13]. This, combined with other parameters – source, stability and chemical composition – led to the identification of AMPs. Based on the limited structural information available at the time, AMPs were referred to as "basic linear peptides" or "basic proteins" [13]. By the early 1980s, there was considerable interest in antimicrobial peptides following the isolation of AMPs from multicellular organisms. Most notably, this included: magainins, from the skin of African clawed frogs [14]; mammalian defensins [15] and cecropins, from the lymph of silk moths [16]. Since then, several hundred AMPs have been identified and classified and details about their potential roles deduced (for an extensive collection you may visit the antimicrobial peptide database at http://aps.unmc.edu/AP/main.php).

AMPs are customarily short (ten to hundred amino acids long) cationic amphipathic peptides [8], which are generally thought to kill cells by disrupting their lipid bilayer membranes; although some likely interact with membranes only in order to gain access to targets inside the cell [1], [17], [18]. Some AMPs may also coordinate innate immune and inflammatory responses, such as: recruitment and accumulation of various immune cells, promoting phagocytosis, prostaglandin release and neutralization of LPS-induced septic shock [1], [19], [20]. Different types of AMPs have very little sequence homology, but share common physiochemical properties, particularly a high proportion of positively charged and hydrophobic residues [21]. They are organized into four motifs: β-stranded, α-helical, loop and extended structure [1]. Over 900 different AMPs have been identified [22], including; thionins, a β-sheet globular AMP found in

plants [1]; cathelicidins, a vertebrate AMP with a well-conserved N-terminal segment that is cleaved for activity [9]; melittin, a very potent AMP found in honey bee venom [9], and many others. In addition, various synthetic AMPs have been produced as an amalgam of two or more natural AMPs – CEME, a cecropin-melittin hybrid [2] – or through modifications of existing AMPs (KSL-W, a modified version of the short AMP KSL) [2]. Understanding the exact mechanisms by which AMPs disrupt lipid bilayers and cell membranes is the subject of extensive research.

In order to determine the mechanism of AMP action, researchers rely on a variety of different techniques; there is no single technique capable of elucidating the mechanism of action on its own. Since their interactions with lipid membranes are key factors in AMP action, solid-state NMR spectroscopy of lipid bilayers has been an important approach to gaining a high-resolution understanding of the mechanism underlying that action [23-25]. Such studies have reported the effects of the AMPs on overall bilayer structure, lipid acyl chain order, and head group tilt, while also providing information on the structure and positioning of the peptide in the bilayer [26]. Such observations provide insight into the interactions of AMPs on bacterial membranes and the effects that membrane and AMP composition have on AMP activity. Solid-state NMR spectroscopy was the method of choice used in this study.

Although not used directly in this project, it is important to note other major techniques that have been applied to the study of peptide-membrane interactions relevant to AMP function. Oriented circular dichroism (OCD) can be used to find the

orientation and secondary structure of AMPs bound to lipid membranes without the need for isotopically labeled material [27]. Differential scanning calorimetry (DSC) can be used to study the effects of AMPs on the organization of lipids in the bilayer [28]. The extent of lipid bilayer disruption by AMPs can be determined by measuring the release of internal florescent-labeled dextran, calcein or other probes [29], [30]. Molecular dynamics (MD) simulations can be used to determine subtle details on AMP-membrane interactions, which would otherwise be hidden using experimental techniques [31]. Other important techniques for studying the mechanism of AMPs include zeta-potential measurements [32], ANS uptake assays [33], atomic force microscopy [34], X-ray diffraction experiments [35], and scanning electron microscope imaging [36].

Using the above-listed techniques, researchers have proposed several mechanisms of AMP-membrane interaction and this is a field of on-going research. In this introduction, I will be focusing on the interactions of α-helical peptides – the most studied group – with the bacterial membrane. The mechanism of AMP action can be divided into three steps: recognition, attachment and membrane disruption [9]. Details of the steps are based on the numerous studies conducted using model membranes to look at peptide-lipid interactions; however, interactions with other components of the bacterial cell envelope such as membrane proteins, peptidoglycan layer, lipopolysaccharide layer, etc. are poorly researched. AMPs display recognition by their ability to preferentially attack bacterial cells at concentrations that leave host eukaryotic cells intact. This recognition is thought to be based in large part on the compositional

differences between the two cells. Bacterial membranes are abundant in anionic phospholipids while eukaryotic membranes predominantly have neutral phospholipids [37]. Thus, the cationic AMPs – composed of cationic amino acids – are strongly attracted to the negatively charged bacterial membrane. Although this electrostatic interaction plays a key role in the selectivity of AMPs, recognition is also influenced by the complexity of bacterial membranes (discussed in detail later). Nonetheless, the outer leaflet of the outer membrane of Gram-negative bacteria is predominantly composed of negatively charged lipopolysaccharides (LPS) [38]. It is believed that cationic AMPs are first attracted to the LPS layer, where they can displace divalent cations of LPS, leading to a self-promoted uptake across the outer membrane and the cell wall; this allows AMPs to gain access to the cytoplasmic membrane [39]. The exact mechanism of this uptake is not well understood, and *ad interim* research has been focused on the binding of AMPs with the cytoplasmic membrane and its subsequent disruption.

Once AMPs have crossed the outer membrane and cell wall, they can bind to the cytoplasmic membrane [37]. This attachment is stabilized by a combination of electrostatic and hydrophobic interactions [40]. AMPs can associate with the cytoplasmic membrane in roughly three different modes. They can either be parallel to the membrane surface (as seen in mellitin) [2]. At an angle to the membrane surface, an orientation adopted by viral fusion peptides, which are found on the viral envelope and mediate viral and host cell membrane fusion [108]. Alternatively, they can also

associate parallel to the membrane normal, as with peptides that mimic transmembrane helices (alamethicin) [2]. Attachment of AMPs is followed by the disruption of the cytoplasmic membrane, which dissipates the electrochemical gradient (necessary for ATP synthesis) leading to cell death. Most AMPs are active against lipid vesicles at high bound peptide to lipid ratios of 1:500 to 1:50 [41].

Following membrane attachment, some AMPs may further enhance their antimicrobial activity either through pore formation – as seen in the barrel-stave or toroidal-pore model – or via a detergent-like carpet mechanism [9]. The exact mechanism of action is dependent on the type and concentration of the AMP involved and the lipid composition of the bilayer it interacts with [23]. These mechanisms need not be mutually exclusive: one process may be an initial or intermediate step and another may be its corollary [23]. Baumann and Mueller (1974) were the firsts to suggest the barrel-stave model of pore formation, based on oriented CD and X-ray scattering experiments of alamethicin in bilayers [42]. With the exception of alamethicin, the barrel-stave model is not believed to be common for AMPs [43]. In the barrel-stave model – one of two models of pore formation – (Figure 1a), AMP monomers initially associate parallel to the membrane surface, whereupon reaching threshold concentrations they reorient themselves into the membrane and aggregate forming a pore [44]. In the AMP aggregate, the hydrophobic residues face the acyl chains of the membrane and the hydrophilic sides form the polar channel [44]. AMPs have to be sufficiently long to traverse the membrane and involve peptide-peptide interactions between the helices in

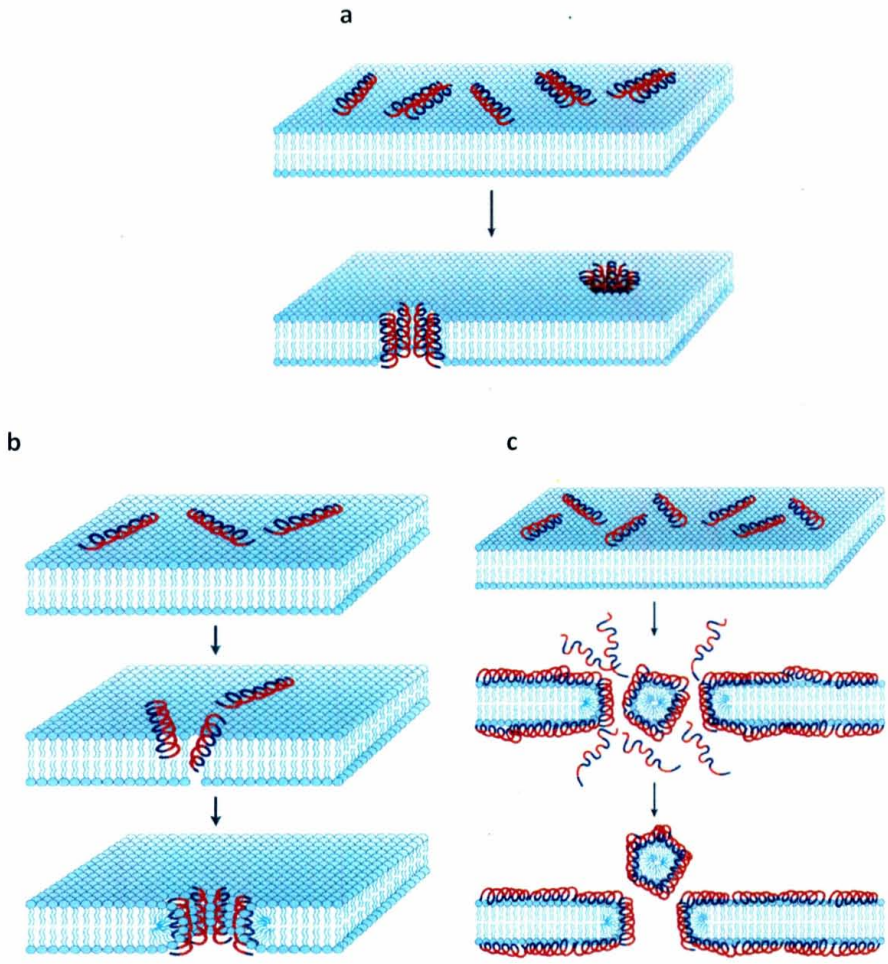

Figure 1. Schematic of models adopted by α-helical AMPs: (a) barrel-stave model, (b) toroidal pore model and (c) detergent carpet like mechanism. Reprinted by permission from Nature Publishing Group: [Nature Reviews: Microbiology] [9], copyright (2005).

the aggregate [44]. Alamethicin, a twenty residue hydrophobic peptide from the fungus *Trichoderma veridae*, is a representative of the barrel-stave model [45]. It forms a channel with eight to nine α-helices per pore and a diameter of approximately eighteen to twenty-six angstroms [45]. There has to be at least twenty-two amino acids in the α-helical conformation in order to span the membrane; however, many AMPs fall well below this prerequisite and cannot form a barrel-stave channel [2].

In order to address AMPs that are too short to traverse the membrane, Ludtke et al (1996), proposed an alternative model of pore formation based on neutron scattering, CD and NMR studies of magainins [45]. This model is referred to as the toroidal-pore model, where the energetically favorable insertion of AMPs into the bilayer causes disruptions in membrane packing and membrane thinning, resulting in a positive curvature of the membrane surface [44]. This allows the bilayer to bend back on itself, connecting the inner and outer leaflets of the membrane and forming a pore composed of both peptides and phospholipids (Figure 1b) [44]. Magainins are well characterized AMPs whose behavior is predicted accurately by the torroidal-pore model; they form pores composed of approximately four to seven monomeric helices with around ninety phospholipids, and have a diameter of approximately thirty to fifty angstroms [45].

A third mechanism of AMP-induced membrane disruption, called the detergent-like carpet mechanism, was suggested by Steiner et al. (1988), who were studying the mechanism of action of cecropins [16]. This model involves the accumulation of AMPs

on the membrane surface (like a "carpet") to a certain threshold concentration. The ensuing disruption of the bilayer leads to the disintegration of the membrane and formation of micelle-like structures, without the establishment of a pore (Figure 1c) [9]. Evidence for this model is provided by infrared spectroscopy studies of cecropin P1, which disintegrates the membrane without significant changes in the order parameter of the acyl chain. This suggests that the peptide does not translocate into the bilayer [46]. It is difficult to distinguish between the torroidal pore and carpet mechanism due to similarities in association of AMPs with the membrane surface; it has been suggested that the torroidal pore could be an intermediate in membrane disintegration [22].

The barrel-stave, toroidal pore and carpet mechanisms have been proposed based exclusively on studies that employ model lipid membranes, i.e. bilayers composed of one or two lipid components. As such, they have failed to take into account the complexity of bacterial cell envelopes (Figure 2). In order to better understand the mechanism of AMP action, a detailed understanding of bacterial physiology and membrane structure and properties is paramount. Bacteria can be classified into two types – Gram-negative and Gram-positive – depending predominantly on the structural organization of their envelope (Figure 2) [47]. Gram-positive bacteria have only one cytoplasmic membrane, while Gram-negative bacteria have two membranes: an outer membrane and a cytoplasmic membrane [47]. Both types have a cell wall composed of peptidoglycan – a polymer of carbohydrates and amino acids – outside of their

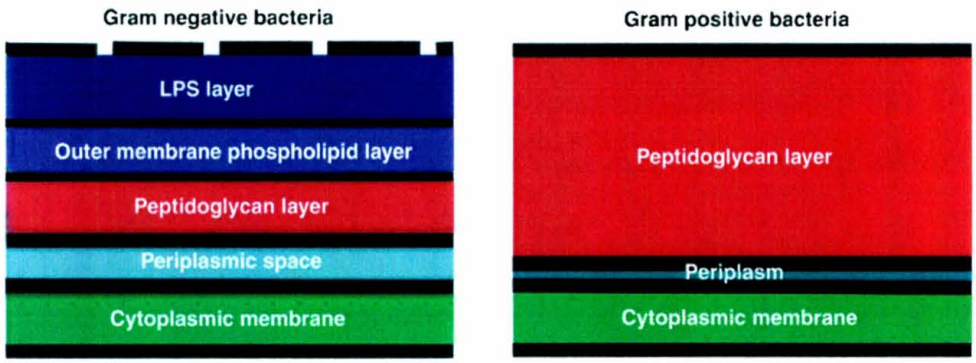

Figure 2. Simple schematic showing the organization of the bacterial envelope in Gram-positive and Gram-negative bacteria. Reprinted by permission from Elsevier: [Biophysical Journal] [73], copyright (2009).

cytoplasmic membrane, which provides structural strength to maintain their shapes [48]. The cell wall in Gram-positive bacteria is much thicker than in Gram-negative bacteria and is often intercalated with polyanionic polymers such as teichoic and teichuronic acids [49]. The two types also differ in terms of lipopolysaccharide composition: Gram-positive bacteria have lipoteichoic acids embedded in the cytoplasmic membrane, while Gram-negative bacteria have LPS (Figure 3d) in the outer leaflet of the outer membrane [50]. The lipid composition of the cytoplasmic membrane can vary depending on the species and the environment [51]. Phosphatidylethanolamine (PE) (Figure 3a), the major zwitterionic lipid, is largely found in Gram-negative bacteria, while Gram-positive bacteria have a very low content of zwitterionic phospholipids [51]. Approximately fifteen percent of the bacterial membrane is comprised of anionic lipids (Figure 3b and 3c) [51] – phosphatidylglycerol (PG) and cardiolipin (CL) – that in part facilitate the selectivity of cationic AMPs towards bacterial cells over eukaryotic cells [9]. Additionally, bacterial membranes also have proteins associated with the lipid bilayer: some proteins span the membrane (transmembrane proteins), while others are attached to the surface via covalent bonds or hydrophobic interactions [38]. There a fewer membrane proteins than lipids but they account for almost half the mass of the membrane and carry out various cellular functions [52]. There is also evidence for the formation of domains in bacterial membranes – lipids undergoing lateral phase separation – including those induced by

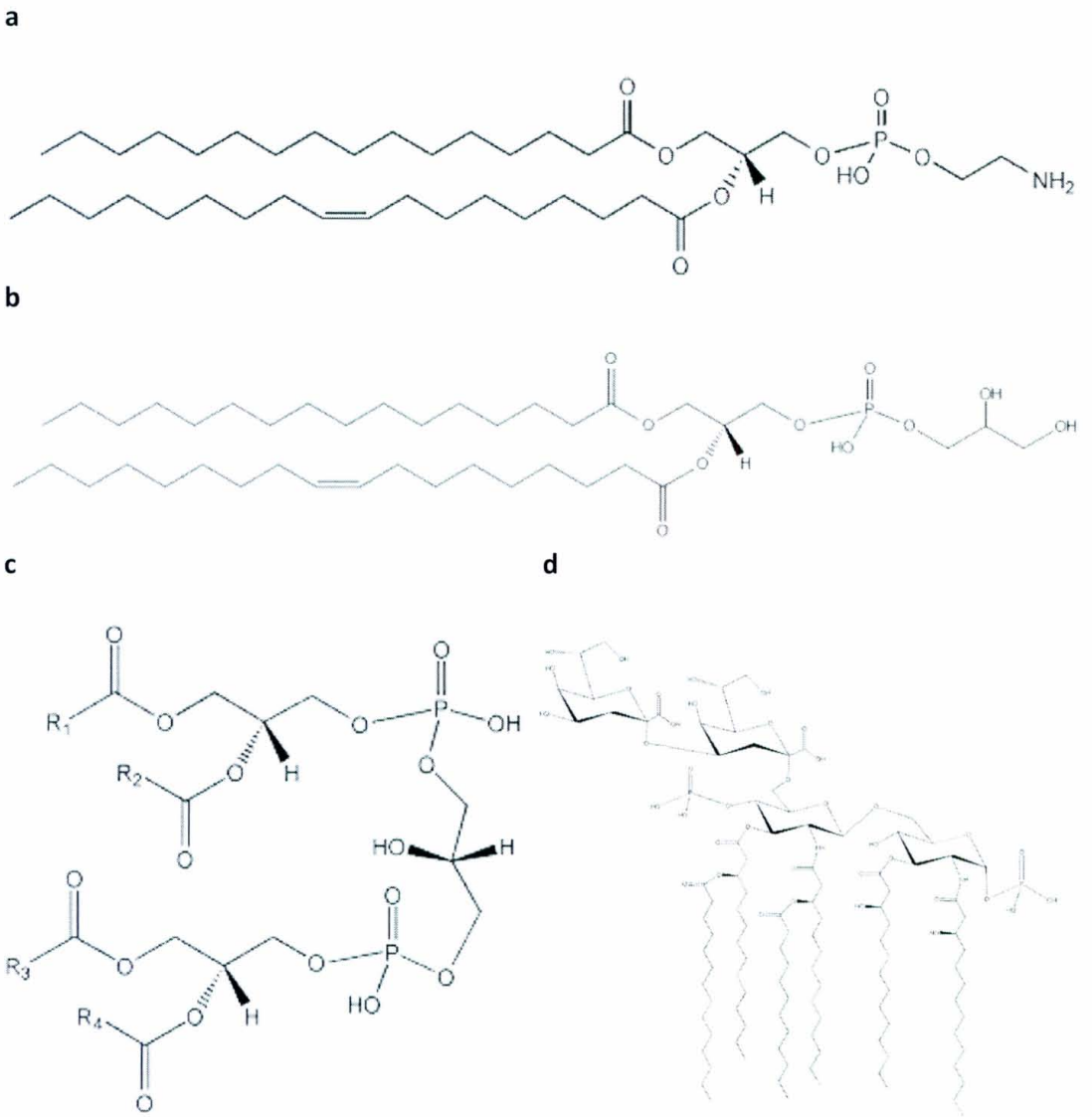

Figure 3. Molecular structures of (a) 1-Palmitoyl-2-oleoyl-*sn*-glycero-3-phosphoethanolamine (POPE), (b) 1-Palmitoyl-2-oleoyl-*sn*-glycero-3-[phospho-*rac*-(1-glycerol)] (POPG), (c) cardiolipin (CL) and (d) lipopolysaccharide (LPS).

polycationic substances such as AMPs [47]. The formation of these domains may alter the stability or composition of the membrane thereby affecting bacterial function [47].

All of these additional components of the bacterial cell envelope may well affect the AMP-bilayer interactions. This possibility has not been addressed by techniques that use model membranes to uncover the mechanisms of bilayer disruption of AMPs. One way to illustrate the enormous gap between the conditions in which biological activity of AMPs are observed and the conditions under which solid-state NMR and other biophysical studies of mechanism are carried out, is to consider the difference in peptide-to-lipid molar (P:L) ratios necessary to induce significant effects in the two circumstances. Solid-state NMR and other biophysical studies on model systems can typically show AMP-induced changes at P:L ratios close to 1:100 (e.g. [71] and [41]). Strikingly, however, a ratio of 100 bacterially-bound peptides: 1 lipid is needed to see inhibition in an *E. coli* sterilization assay, i.e. ten thousand times more peptide per lipid [41]. At the other extreme, some researchers have wondered how AMP concentrations high enough to have an impact are achieved *in vivo*, and have attempted to provide an explanation based on the high membrane-bound concentrations of AMPs that can be achieved even at relatively low solution concentrations [53].

While there is a body of work substantiating the "self-promoted uptake" mechanism by which AMPs may traverse the outer membrane of bacteria (e.g. [54]), and though a handful of solid state NMR studies of AMPs have been performed with

bacterial lipid extracts (e.g. [55]), to our knowledge there was no published work that applies high resolution techniques such as NMR to the study of AMPs in intact bacteria.

In order to bridge the gap between the NMR studies of AMPs using model membranes with the functional mechanism occurring in intact cells, one approach is to conduct ^{2}H NMR studies of entire bacteria. Ideally for such studies, the ^{2}H labels should be incorporated at high levels into the lipids of the bacterial membrane, without any ^{2}H being incorporated into other parts of the cell that would give undesirable background signal. In order to accomplish this goal, it was necessary to manipulate the pathways involved in bacterial membrane lipid biosynthesis and metabolism.

Bacteria have the ability to modify their membrane lipid composition by modifying the type of fatty acids they synthesize. Most bacteria display a type II fatty acid biosynthetic pathway (Figure 4) – characterized by predominantly discrete monofunctional enzymes – where synthesis takes place in the cytosol [56]. Initiation of fatty acid synthesis begins with the conversion of acetyl-CoA to malonyl-CoA by acetyl-CoA carboxylase (ACC) [57]. ACC is a heterotetramer encoded by four genes: *accA*, *accB*, *accC* and *accD* [57]. Malonyl-CoA is the ketone intermediate, which adds 2 carbon units to a growing acyl chain through a series of reactions catalyzed by various fatty acid synthases [58]. Reactions catalyzed by the fatty acid synthases can produce fatty acids of varying lengths and degrees of saturation. Following fatty acid synthesis, acyltransferases in the membrane can recognize specific fatty acid end products and transfer them to glycerol-3-phosphate, eventually leading to the formation of

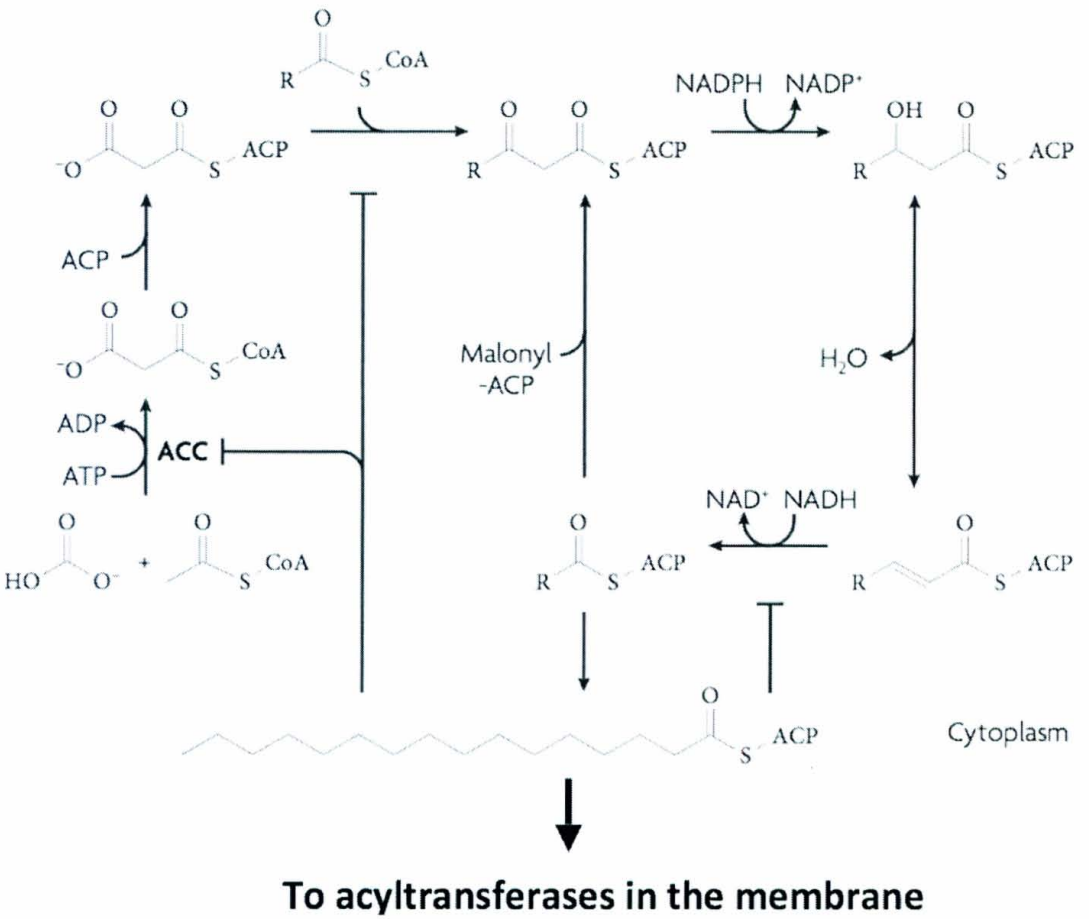

Figure 4. Simple schematic showing the phospholipid biosynthetic pathway in *Escherichia coli*. Modified and reprinted by permission from Nature Publishing Group: [Nature Reviews: Microbiology] [58], copyright (2008).

membrane phospholipids [59]. Bacteria also have the ability to break down fatty acids into acetyl-CoA units, which can then be used in other pathways involving energy metabolism, carbohydrate and amino acid synthesis [60]. Fatty acid breakdown is accomplished via the β-oxidation cycle, where the first and a key step in fatty acid breakdown is carried out by an acyl-CoA dehydrogenase encoded by the *fadE* gene [61]. Commonly, researchers have used lipid mutants of *E. coli* in order to study membrane biosynthesis [62], [63]. One such mutant was the K1060 strain, which is a fatty acid auxotroph that is unable to synthesize or degrade unsaturated fatty acids [64]. In order for this strain to be viable, unsaturated fatty acids needed to be supplemented in its growth media [64]. In this work, this mutant was initially used in order to selectively label the unsaturated chain via incorporation of ^{2}H-labeled oleic acid in the growth media. Thus, K1060 can be used for ^{2}H NMR studies of the unsaturated chain. However, the interpretation of studies based on this strain might be limited by the fact there are very few published ^{2}H NMR studies on the unsaturated chain (e.g. [65]), with which to compare my results.

On the other hand, ^{2}H NMR studies on the saturated chain of model membranes are extensive (e.g. [66], [67], [68] etc.) and ^{2}H NMR studies of the saturated chains in the context of entire bacteria would be most beneficial for comparison. Unfortunately, no commercial strains were available that would allow incorporation of labeled saturated chains into the membrane. In order to overcome this obstacle, I created a new strain of *E. coli*, termed LA8. This was done by modifying *E. coli* strain L8, which already has a

mutation that affects total fatty acid synthesis (*accB*) [69], to also be deficient in fatty acid metabolism, via a mutation in *fadE*. The combined effects of these modifications allow for the incorporation of labeled saturated fatty acids specifically into the membrane by supplementing them into the growth media.

For this study, I chose to treat the ^{2}H-membrane-labelled *E. coli* with a well studied, highly active AMP. MSI-78 (Figure 5) is a synthetic peptide analog of magainin 2 that is found in the skin of bullfrogs [70]. It is a very potent hydrophilic antibiotic with an MIC value of 4 μg / cell, a net cationic charge of 9 and a grand average hydropathicity index of -0.159 [71]. MSI-78 is unstructured in aqueous medium but adopts a helical conformation when it interacts with membranes [72]. NMR studies indicate that it tends to be oriented nearly perpendicularly with respect to the bilayer normal, inducing a positive curvature strain on lipid bilayers consistent with formation of torroidal pores [71].

Four main objectives were established and completed in this study. The first objective was to determine if ^{2}H NMR studies of entire bacteria in the presence of AMPs was achievable. To do so, I used an existing strain (K1060) and determined the effects media and processing had on the ^{2}H NMR spectra. The second objective was to engineer a novel strain (LA8) specifically designed for ^{2}H NMR studies. Using this novel strain, I determined the appropriate conditions required to achieve good quality ^{2}H NMR spectra. The third objective was to further characterize this novel strain using cell

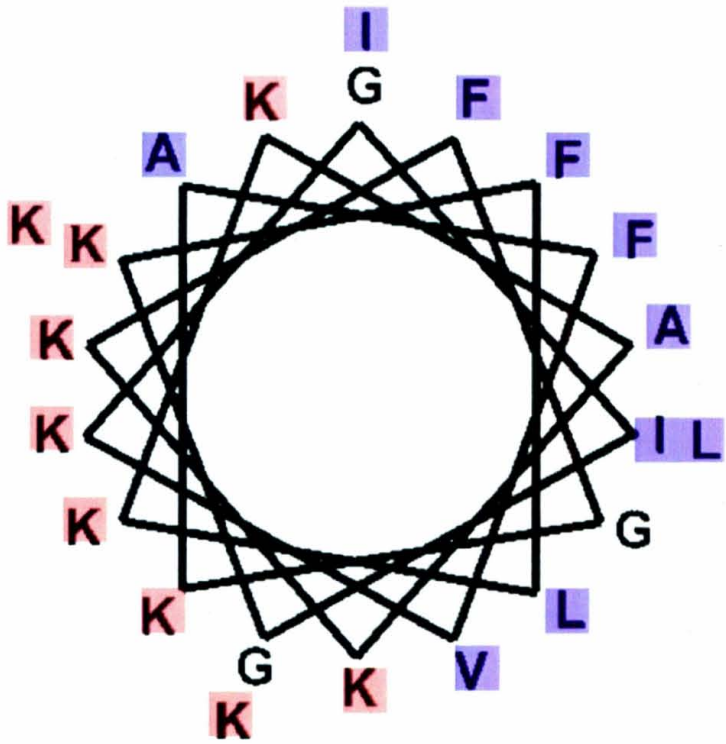

Figure 5. Helical wheel representation of MSI-78. Amino acid residues highlighted in red are cationic and those highlighted in blue are hydrophobic. Modified and reprinted by permission from Elsevier: [Biophysical Journal] [71], copyright (2006).

2. Materials and Methods

2.1 Peptide synthesis and purification

MSI-78 (NH_2-GIGKFLKKAKKFGKAFVKILKK-NH_2), was synthesized with help from Donna Jackman (Booth lab, Biochemistry, MUN) via solid-phase synthesis using O-fluorenylmethyloxycarbonyl (Fmoc) chemistry. Organic solvents and other reagents used for synthesis and purification were purchased from Sigma-Aldrich Co. (St. Louis, MO). The peptide was synthesized using a CS336X peptide synthesizer (CS Bio Co., Menlo Park, CA) following manufacturer's instructions. Fmoc amino acids (CS Bio Co., Menlo Park, CA) were weighed out in 5X excess and placed in tubes on the peptide synthesizer. The synthesizer used a prederivatized Rink amide resin to assemble the peptide. Dissolution of amino acids was carried out using 0.4 M 1-hydroxy-benzotriazole (HoBt) dissolved in dimethylformamide (DMF). De-blocking and resin washes were accomplished using a 20% piperidine/DMF solution and DMF, respectively. At completion of synthesis, the resin with the assembled peptide was transferred to a 10 ml syringe equipped with a filter and washed thoroughly with methanol under vacuum. The resin was then air dried for 30 min and then under vacuum for 60 min. Cleavage of the peptide from the resin was carried out by the addition of trifluroacetic acid solution (TFA) (95% by volume), which was stirred for 3 h and then transferred to a 50 ml Falcon tube (Greiner Bio-One, Monroe, NC). The peptide was then cold precipitated using 50 ml of diethyl ether at -20°C. The precipitate was pelleted by centrifugation (2000 × g at -4°C

for 5 min), re-suspended in double distilled water with 0.1% TFA and filtered to remove undissolved particulate.

Purification of the peptide was carried out using high-pressure liquid chromatography (HPLC) (Varian ProStar HPLC, Varian Inc., St. Laurent, QC). The HPLC was equipped with a reversed phase Vydac C-8 column and made use of a water/acetonitrile linear gradient. Peptides were detected via UV spectroscopy at a wavelength of 215 nm. The strongest (highest absorbance in milli-absorbance units (mAU) at 215 nm) peak on the HPLC chromatograph (Figure 6) was collected, and its mass analyzed. The molecular weight of the peptide samples was confirmed via matrix-assisted laser desorption/ionization-time of flight mass spectrometry (MALDI-TOF MS) at the Genomics and Proteomics (GaP) facility (Memorial University, St. John's, NL). Upon confirmation of the desired peptide, the sample was lyophilized and stored at 4°C. For NMR experiments, 10-mg/ml stock solution of MSI-78 in Medium 63 (Table 2) was prepared and exact volumes added to bacterial samples as needed.

2.2 Bacterial strains used and media preparation

Bacterial strains and plasmids used in this study are listed in Table 1. All strains were grown in a shaking incubator at 170 rpm. Strain BW25141/pKD4 from the Coli Genetic Stock Center (CGSC, Yale University, New Haven, Conn.) was used to obtain the pKD4 plasmid (carrying the *kan* gene). The strain was grown at 37°C in Luria–Bertani (LB) medium (5 g/l NaCl, 5 g/l yeast extract and 10 g/l tryptone) supplemented with 50 μg/ml of kanamycin (Sigma-Aldrich, St. Louis, MO). Strain BW25141/pKD46 from the

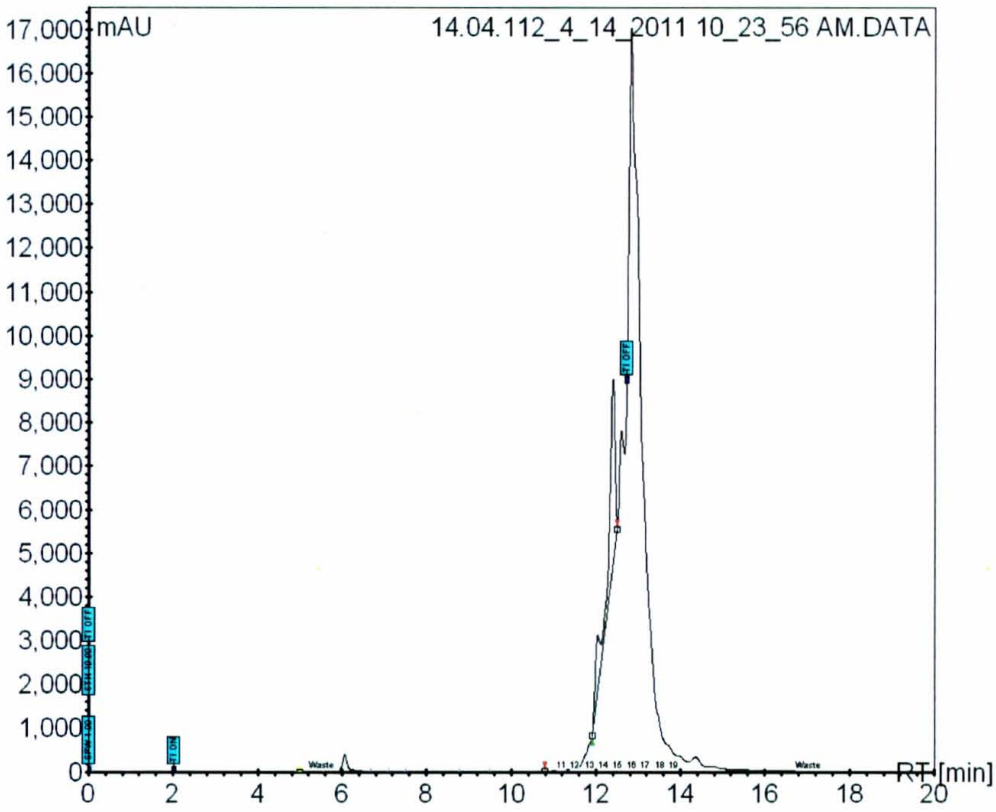

Figure 6. HPLC spectrum of MSI-78 eluted with an acetonitrile gradient. Samples were run through a preparatory reverse-phase HPLC chromatographer equipped with a Vydac C-8 column. The strongest [highest absorbance in milli-absorbance units (mAU) at 215 nm] peak (≈12.8 min) was extracted and confirmed to have a mass consistent with MSI-78 by MALDI-TOF-MS.

Table 1. Strains and Plasmids used in this study.

Strain	Relevant Genotype	Source
K1060	F', *fadE62, lacI60, tyrT58(AS), fabB5* and *mel-1*	CGSC
L8	F-, *araC14, lacY1, tsx-57, glnV44(AS), gltA5, galK2(Oc), Rac-0, accB22(ts), rpsL20(strR), xylA5, mtl-1, lldD1, thi-1* and *tfr-5*	CGSC
LA8	F-, *araC14, lacY1, tsx-57, glnV44(AS), gltA5, galK2(Oc), Rac-0, accB22(ts), rpsL20(strR), xylA5, mtl-1, lldD1, thi-1, tfr-5* and *ΔfadE::kan*	Created in lab
Plasmid		
pKD4	Template vector, *oriR6Kgamma, bla(ApR), rgnB(Ter), kan, FRT* and *bla*	CGSC
pKD46	Expression vector, *repA101(ts), araBp-gam-bet-exo, oriR101, bla(ApR), araC, bla* and *[tL3]*	CGSC

CGSC was used to obtain the pKD46 plasmid (carrying the λ Red genes). The strain was grown at 30°C in LB medium supplemented with 100 μg/ml of ampicillin (Sigma-Aldrich, St. Louis, MO). The plasmids were then isolated using the PureYield Plasmid Miniprep System (Promega, Madison, WI) according to the manufacturer's instructions. All other bacterial cultures were grown in Medium 63 [74] supplemented with appropriate nutrients as listed in Table 2. Solid medium plates were prepared using the appropriate liquid media + 1.5% agar.

2.3 K1060 E. coli *sample preparation for ^{2}H NMR studies*

The filter paper disk carrying the K1060 strain from the CGSC was placed in LB medium, supplemented with 50 μg/ml of oleic acid and grown overnight at 37°C. The resulting culture was spread on a solid medium plate containing LB and 50 μg/ml of oleic acid and incubated overnight at 37°C. A well-isolated colony was then selected and cultured in liquid media (LB + 50 μg/ml of oleic acid) and grown overnight at 37°C. The resulting culture was stored as 1 ml aliquots in 50% glycerol at -80°C, until needed.

To produce bacteria for deuterium NMR observation of labeled unsaturated chains (deuterated oleic acid), 100 ml of Medium 63-C (glucose as carbon source) or Medium 63-D (casamino acids from casein protein as carbon source) was inoculated with the K1060 strain. These cells were grown at 37°C in a 500 ml Erlenmeyer flask using a shaking incubator (Shel lab, Cornelius, Oregon) at 150 rpm. The cells were then harvested in the stationary phase (A_{600} of ≈2.0) and transferred into two sterile 50 ml

Table 2. Media used in this study.

Medium	Nutrients
Medium 63	13.6 g/L KH_2PO_4, 2.0 g/L $(NH_4)_2SO_4$, 0.2 g/L $MgSO_4.7H_2O$, 0.5mg/L $FeSO_4.7H_2O$, 4.0 g/L glycerol and adjusted to pH 7.0 with KOH
Medium	**Medium 63 supplemented with**
Medium 63-A	1 µg/mL thiamine, 3 g/L casamino acids and 30 µg/ml kanamycin
Medium 63-B	1 µg/mL thiamine, 3 g/L casamino acids, 1 g/L Brij-58, 50 µg/mL deuterated palmitic acid, 50 µg/mL oleic acid and 30 µg/ml kanamycin
Medium 63-C	1 µg/mL thiamine, 2 g/L glucose, 1 g/L Brij-58 and 50 µg/mL deuterated oleic acid
Medium 63-D	1 µg/mL thiamine, 3 g/L casamino acids, 1 g/L Brij-58 and 50 µg/mL deuterated oleic acid
Medium 63-E	1 µg/mL thiamine and 3 g/L casamino acids
Medium 63-F	1 µg/mL thiamine, 3 g/L casamino acids, 1 g/L Brij-58, 50 µg/mL oleic acid and 50 µg/mL palmitic acid

Falcon centrifuge tubes. The cells were centrifuged at 4°C for 10 min at 4100 × g, after which the cells were washed two times in cold Medium 63 containing 0.1% Brij-58. The sample was centrifuged again (4°C for 10 min at 4100 × g) and the pellet with labeled unsaturated chains was used immediately for ^{2}H-NMR studies. Each sample occupied a volume of ≈500 µl and had the viscosity of a paste. For samples containing no peptide, approximately two hours elapsed between the initial harvesting of cells and the beginning of the NMR experiment.

^{2}H NMR studies of bacteria treated with peptide required some additional preparative steps. After the washing and centrifugation step described above, the pellet was re-suspended by gentle agitation in 100 ml of Medium 63 for 15 min. Then an appropriate amount of peptide was added and the sample vortexed thoroughly for ≈10 sec. This sample was then centrifuged as above and used for NMR. Samples were transferred into the NMR sample holder using a sterile spatula. Control experiments with buffer (Medium 63) in place of AMP were also carried out. For these controls, samples were prepared as described above in order to test for any effect of vortexing. For the peptide samples, approximately 2.5 h elapsed between the initial harvesting of cells and the beginning of the NMR experiment.

The peptide concentration for each sample is expressed as %w/w (peptide/dry cell weight). To measure the dry weight of bacteria, samples were grown to an A_{600} ≈2.0 and processed in the same manner as described above. The resulting pellet was then dried under vacuum for 48 hours and weighed on an analytical balance. The average of

the measured weights was used as the theoretical dry cell weight in samples containing peptide.

2.4 Engineering the LA8 bacteria

To create the LA8 strain, Pfu DNA polymerase (Stratagene) and GenElute Bacterial Genomic DNA Kit were purchased from Cedarlane (Burlington, ON) and Sigma-Aldrich (St. Louis, MO), respectively. Plasmid DNA purification and PCR purification were performed using spin column kits purchased from Promega (Madison, WI) following the manufacturer's instructions. A MicroPulser Electroporator from Bio-Rad (Hercules, CA) was used for linear DNA transformations. L-arabinose used for induction was purchased from Sigma-Aldrich (St. Louis, MO).

In creating the LA8 strain, genetic manipulations were performed on the L8 strain in order to replace the *fadE* gene (needed for fatty acid metabolism) with a kanamycin resistance gene, using the method of Datsenko and Wanner [75] as outlined in Figure 7. The L8 strain was first transformed with the pKD46 plasmid, which encodes the λ Red genes (γ, β and exo) under the control of an arabinose-regulated promoter [76]. This plasmid also expresses ampicillin resistance as a selection marker [76]. In order create the transformant, the L8 strain was grown at 30°C in Medium 63-E overnight (≈16h), subcultured at 37°C in fresh Medium 63-F and grown to A_{600} of ≈0.6. One hundred microliters of the cells were transferred to a 1.5 ml Eppendorf tube and incubated on ice for 10 min. Fifty nanograms of the pKD46 plasmid was added to the

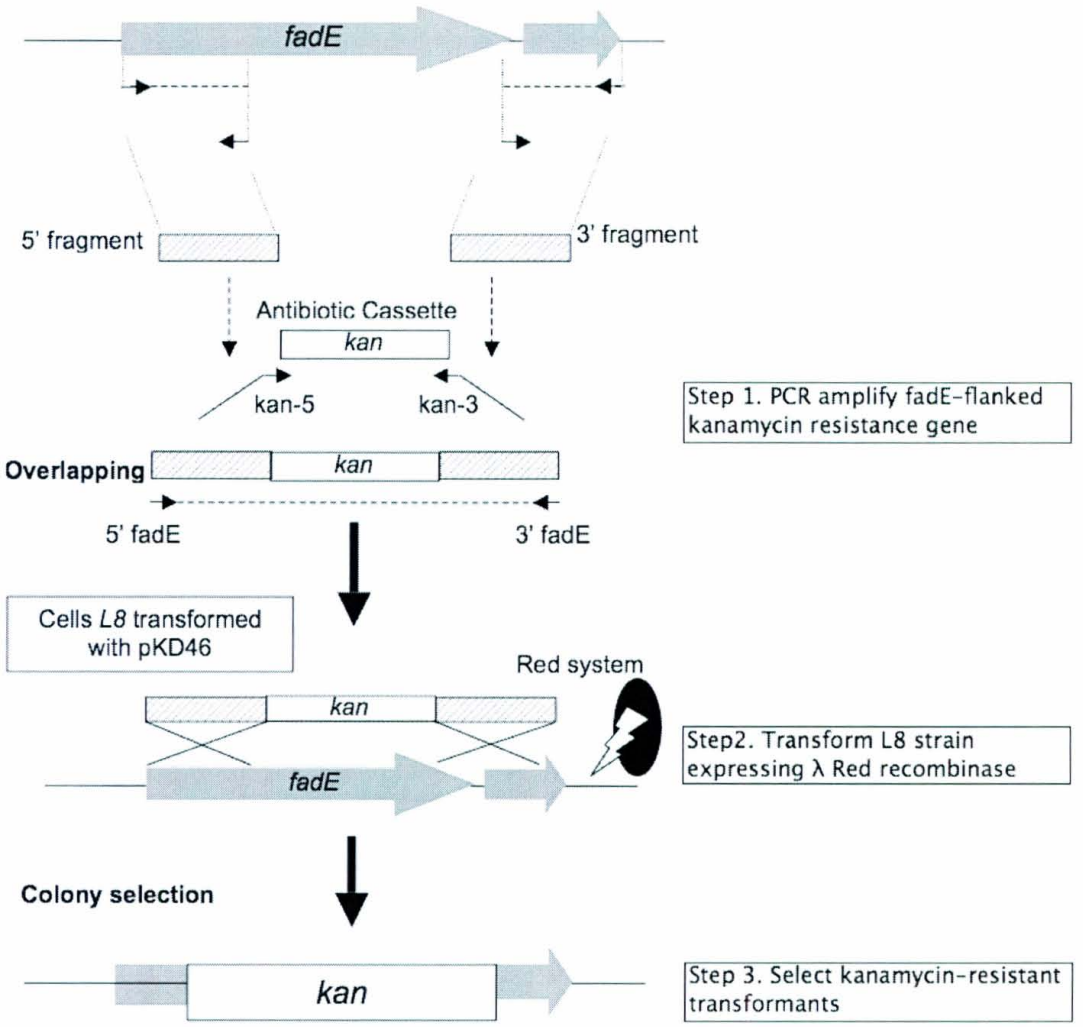

Figure 7. λ Red recombinase strategy of Datsenko and Wanner (2000) [75] used to create the LA8 strain.

Eppendorf tube and allowed to incubate for another 10 min. The tube containing the L8 strain and pKD46 plasmid was then heat shocked in a hot water bath at 42°C for 45 seconds followed by 2 min on ice. One milliliter of Medium 63-F was added to the tube, which was then incubated for 1 hour at 37°C. One hundred microliters of the resulting culture was spread on an agar plate containing Medium 63-F and 100 μg/ml of ampicillin and grown overnight (≈16h) at 37°C. Ampicillin-resistant transformants were selected for and cultured in liquid media (Medium 63-F) and grown overnight at 37°C. The resulting culture was stored as 1 ml aliquots in 50% glycerol at -80°C, until needed. These transformants are referred to as L8/pKD46.

pKD4 [75] encoding the kanamycin resistance gene (*kan*) between the P1 and P2 site was used as a template for PCR amplification of the *kan* gene. The following reagents were used for PCR amplification: 2.50 U Pfu DNA Polymerase, 30 ng of pKD4, 0.2 μM of each primer (KAN-f & KAN-r) (Table 3), 250 μM of each dNTP and 1.0X PCR buffer. Primers were designed based on the sequences of the *kan* and *fadE* genes and synthesized by Sigma-Aldrich (St. Louis, MO). The cycling parameters used for the PCR reaction were: an initial denaturation period of 5 min at 95°C, 35 temperature cycles (94°C for 45 sec, 52°C for 45 sec and 72°C for 90 sec), followed by a final 10 min interval at 72°C. The final PCR product was purified and stored at -20°C in nuclease-free water until needed. The synthesized linear PCR product contains the *kan* gene, which is flanked by sequences homologous to the start and stop regions of the *fadE* gene. To prepare electrocompetent L8/pKD46 cells, the strain was grown at 30°C in Medium 63-E

overnight. One milliliter of the overnight culture was then added to 100 ml of Medium 63-F supplemented with 50 µg/ml of ampicillin and 10 mM of L-arabinose. The bacterial culture was then incubated at 30°C and grown to an A_{600} of ≈0.6. The culture was chilled on ice for 10 min and then centrifuged at 4°C for 10 min at 4100 × g. The resulting pellet was washed twice with ice-cold 10% glycerol and then re-suspended in 5 ml of ice-cold glycerol (concentrated 20-fold). The now electrocompetent L8/pKD46 cells were distributed into 50 µl aliquots and stored at -80°C until needed.

For the electroporation, an aliquot of electrocompetent cells were thawed on ice and mixed with 10 to 100 ng of the linear PCR product containing the *kan* gene. The mixture was then transferred to a chilled 0.2 cm electroporation cuvette (BioRad, Hercules, CA) and shocked once at 2.5 kV (Dr. Andrew Lang generously provided the electroporator and corresponding cuvettes). One milliliter of Medium 63-F was added to the shocked cells and quickly transferred to a sterile culture tube and incubated at 37°C for 2 hours with moderate shaking. Aliquots of the culture were then plated on selective medium containing 30 µg/mL kanamycin. Kanamycin-resistant colonies were isolated and cultured in liquid media (Medium 63-B) and grown overnight at 37°C. The resulting culture was stored as 1 ml aliquots in 50% glycerol at -80°C, until needed. Successful recombinants contained the *kan* gene in place of the *fadE* gene; these recombinants will be referred to henceforth as LA8.

The presence of the *kan* gene in the proper orientation in these mutants (LA8) was confirmed via PCR. The LA8 bacterial genome was isolated using the GenElute Bacterial

Genomic DNA Kit. Once isolated, the region corresponding to the *fadE* gene was amplified using FadE-f and FadE-r primers (Table 3). The linear PCR product was sequenced at the Genomics and Proteomics Facility (GaP) (Memorial University, St. John's, NL) to confirm the presence of the *kan* gene.

2.5 LA8 E.coli *sample preparation* ^{2}H *NMR studies*

For NMR experiments, strain LA8 was grown at 30°C in 10 ml of Medium 63-A (Table 2) overnight (without fatty acid supplements) and subcultured in 400 ml of fresh Medium 63-B (supplemented with fatty acids including deuterated palmitic acid). The cells were then grown at 37°C in a 4000 ml Erlenmeyer flask using a shaking incubator at 150 rpm. The cells were grown to the mid-log phase (A_{600} of 0.6-1.0) and then harvested by centrifugation at 4°C for 10 min at 4100 × g. For studies of untreated cells, the bacteria were then washed either once or twice with gentle agitation for 15 min in 100 ml of Medium 63 containing 0.1% Brij-58. The sample was centrifuged as before and the pellet with labeled saturated chains was then used immediately for ^{2}H-NMR studies. Each sample occupied a volume of ≈500 µl and had the viscosity of a paste. For the peptide-free sample, it takes approximately 1.5h or 2h (washed once or twice, respectively) between the initial harvesting of cells and the beginning of the NMR experiment.

For bacteria treated with peptide, additional steps were carried out. After the washing (only done once) and centrifugation step described above, the pellet was

used for the spectrometers were 61.42 MHz and 23.2 MHz, respectively. Both spectrometers were assembled in-house and included: a pulse programmer, a quadrature detector, a 1000W amplifier and a computer for data collection. The NMR probe head was an in-house assembled apparatus that enclosed the radio frequency coil and the sample. The temperature in the probe was controlled to ± 0.1°C using a LakeShore Cryogenics (Westerville, OH) temperature controller. Data collection and analysis was done using a NMR program (MEMNMR v 3.0) written in house.

To obtain ^{2}H-NMR spectra of bacterial cells, a quadrupole echo pulse sequence ($\pi/2$-τ-$\pi/2$-acq) was used as described elsewhere [77], with a 900 ms recycling delay, a 30 μs pulse separation and a 5 μs pulse duration. Data were collected using a 1 μs dwell time and a free-induction-decay length of 8192 points. Oversampling by a factor of 4 was applied to give an effective dwell time of 4 μs [78]. The free induction decay was left-shifted to place the echo maximum as the first point. To check for sensitivity of the observed signal to pulse parameters, NMR experiments were also performed using the above parameters but with 500 ms recycling delay and either a 40 μs or 60 μs pulse separation. Depending on the signal strength, 8000 to 172000 scans were averaged. To monitor time-dependent changes in the spectral shape, transients were averaged in sequential blocks of 8000 scans, each collected over 2 hours. When comparing samples containing different peptide concentrations for the LA8 strain, 32000 transients were

averaged for each spectrum displayed. For moment calculations, the imaginary channel was zeroed before Fourier transformation, in order to symmetrize the spectra.

Echo decay times (T_{2e}) were measured for each sample by varying the quadrupole echo sequence pulse separation, τ, sequentially from 30 to 400 μs. For each pulse separation, 2000 transients were averaged to obtain the echo amplitude. The mean echo decay rates, $<1/T_{2e}>$, were obtained from fits to the initial echo decay according to

$$A_0(2t) = A_0(0)e^{-2t\langle 1/T_{2e}\rangle} \qquad (1)$$

where A_0 is the maximum amplitude of the echo. The reported echo decay times are the inverse of the mean echo decay rate [79].

2.7 Moment Analysis

First spectral moments (M_1) were calculated from the symmetric ^{2}H-NMR powder pattern spectra according to

$$M_2 = \frac{\int_0^\infty \omega^2 f(\omega)\, d\omega}{\int_0^\infty f(\omega)\, d\omega} \qquad (2)$$

where ω is the frequency with respect to the central Larmor angular frequency ω_o and $f(\omega)$ is the line shape [80]. The first moment is proportional to the average quadrupole splitting in the spectrum and thus to the average of the deuteron orientational order parameter

$$S_{CD} = \frac{1}{2}\left\langle 3\cos^2\theta - 1 \right\rangle \qquad (3)$$

over the deuterated chains. In Eq. 3, θ is the angle between the CD bond on a given chain segment and the bilayer normal, which is the axis about which the chain undergoes fast, axially symmetric reorientation [81].

Second spectral moments, M_2, were also calculated from the symmetric powder patterns according to

$$M_2 = \frac{\int_0^\infty \omega^2 f(\omega)\, d\omega}{\int_0^\infty f(\omega)\, d\omega} \qquad (4)$$

Second moments were used to calculate the parameter

$$\Delta_2 = \frac{M_2}{1.35 \times M_1^2} - 1 \qquad (5)$$

which is the relative mean square width of the distribution of orientational order parameters [80] and is sensitive to the shape of the spectrum.

For each spectrum, baselines for the integrals in Eqs. 2 and 4 were obtained by averaging all points in the range 33.6-45.8 kHz. For samples with no peptide, integrals ran from 0 kHz to 29.3 kHz. For peptide-containing samples, intensity reaches the baseline at smaller frequencies and the integrals were cut off at 24.4 kHz. For all spectra, the narrow feature at the spectral centre – corresponding to isotropically-reorienting natural abundance deuterated water – was clipped between +/- 0.4 kHz by setting the intensity in that range to the average of the intensity in the range 0.4-0.5

kHz.

2.8 Cell viability: Spread plate count

Plate counts were performed on samples in pre-NMR and post-NMR conditions. In this context, pre-NMR refers to the state of the raw bacterial culture before it has been processed and placed in an incubator. Post-NMR refers to the sample that has been processed (described in section 2.5) and placed in an incubator at 37°C for various durations (mimicking conditions of an NMR experiment).

For pre-NMR counts of colony forming units (CFUs), 4 tubes were filled with 9.0 ml of sterile Medium-63. One milliliter of the stock culture was transferred aseptically to the first tube and vortexed to give a 1:10 diluted culture. One milliliter of the diluted culture was then transferred aseptically to the second tube with sterile Medium-63. The second tube was vortexed to give a 1:100 diluted culture. The above steps were repeated in series with the third and fourth tube to give 1:1000 and 1:10000 diluted cultures. One hundred microliters of each diluted culture was pipetted onto the appropriate solid medium plate and spread over the entire plate using a sterile glass spreader. For each diluted culture, plates were prepared in triplicate and incubated at 37°C overnight. The next day, only plates with between 30 and 300 CFUs were used in the plate counts. For each set of diluted cultures the number of CFUs were averaged and used in all subsequent percent viability calculations. The solid medium plate used for the K1060 strain was either Medium 63-C or Medium 63-D, and for the LA8 strain it was Medium 63-B.

Post-NMR counts of CFUs involved an additional step before continuing with the steps listed above. The bacterial sample was first re-suspended in sterile Medium 63 to a final volume that was the same as the original stock culture. The sample was then processed in the same manner as the pre-NMR sample and the CFUs determined. The cell viability was expressed as a percentage of the CFUs post-NMR to pre-NMR for the various time intervals. For the same time intervals, cell viability was also expressed as a percentage of the CFUs post-NMR relative to a sample immediately after processing.

2.9 Cell viability: MTT reduction assay

MTT reduction assays were performed for pre-NMR and the corresponding post-NMR samples. This cell viability assay is based on the method of H. Wang et al. [82]. A stock solution of 3-(4,5-dimethylthiazol-2-yl)-2,5-diphenyl tetrazolium bromide (MTT) was prepared in distilled water to a concentration of 5.0 g/l and stored at -20°C until needed.

LA8 bacteria were harvested in the mid-log phase at an A_{600} ≈0.6. One-and-a-half milliliters of the culture were set aside and the rest of it processed in the same manner as used for the NMR experiments (Section 2.4). The 1.5 ml cell culture was then centrifuged at 10000 × g for 30 sec and then re-suspended in 1.5 ml of fresh Medium 63. The cell suspension was then diluted (1:10) in Medium 63 and 200 µl of the diluent transferred into 1.5 ml centrifuge tubes. Twenty microliters of the thawed MTT stock solution was added to the diluted bacterial culture and thoroughly mixed in order to

initiate the reduction reaction. The mixture was then incubated at 37°C for 20 min. The bacteria-formazan crystal complexes that formed were then collected by centrifugation at 10000 × g for 30 sec. The pellet was then transferred into test tubes using 2.5 ml of DMSO and thoroughly mixed. After 10-15 min, the absorbance was measured at 550 nm. For each sample the MTT assay was performed in duplicates.

For post-NMR conditions, the sample was first re-suspended in sterile Medium 63 to a final volume that was the same as the original stock culture. The sample was then processed in a similar fashion as the pre-NMR sample and the A_{550} was measured. The cell viability was expressed as a percentage of the A_{550} post-NMR to pre-NMR for the various time intervals. For the same time intervals, cell viability was also expressed as a percentage of the A_{550} post-NMR relative to a sample immediately after processing.

2.10 Minimal inhibitory concentration (MIC) assay

The minimal inhibitory concentration (MIC) of MSI-78 was determined against the LA8 strain and the laboratory control JM109 strain (Invitrogen, Grand Island, NY). Using a modified version of the growth method described by Wiegand et al. [83], 10 ml each of Medium 63-F and Medium 63-E were inoculated with the LA8 and JM109 strains, respectively. The cells were then grown at 37°C to an $A_{600} \approx 0.6$. 1.0 ml of each bacterial culture was transferred aseptically to a tube with 9.0 ml of each strain's respective growth media. The tubes were then vortexed to give a 1:10 diluted culture of each strain. The above dilution steps were repeated in series to produce a 1:1000

diluted culture of each strain. The resulting diluent had a working concentration of ≈5 X 10^5 CFUs/ml for each strain.

Lyophilized MSI-78 was dissolved in Medium 63 to produce a stock solution at a concentration of 1 mg/ml. Twenty µl of the stock MSI-78 solution was pipetted into column 1 of a 96-well round-bottom polypropylene plate (Corning Inc., Corning, NY). Twenty microliters of Medium 63 alone was also added to column 1 to determine any antimicrobial effects of the buffer itself. Ten microliters of Medium 63 was then added to all wells from columns 2-10. In order to obtain a two-fold dilution, 10 µl from each well in column 1 was added to the corresponding well in column 2, and the resulting solutions were mixed by pipette. The above steps were repeated in series until column 10, where the excess 10 µl was discarded. This resulted in 10 solutions of MSI-78 with concentrations ranging from 100 µg/ml to 0.20 µg/ml, decreasing by a factor of 0.5 from columns 1-10.

Using a second 96-well round-bottom polypropylene plate, 90 µl of each bacterial culture (diluted 1:1000) was pipetted in duplicate into columns 1-10, and 100 µl into column 11 as a growth control. As a sterility control, 100 µl of Medium 63-F and Medium 63-E – growth media of LA8 and JM109, respectively – were pipetted into column 12. Ten microliters from each of the wells containing the peptide solution from column 1-10 was transferred to the corresponding wells in the plate with the bacterial culture. The plate was then sealed with breathable sealing tape and incubated at 37°C overnight (≈16 h). To confirm the correct working concentration of each bacterial

culture, 10 µl was removed from the growth control well for each strain and transferred into 990 µl of Medium 63. The sample was then vortexed to produce a 1:100 dilution. A 1:1000 dilution was made by pipetting 100 µl of the 1:100 diluent into 900 µl of Medium 63. Both of the dilutions were plated onto solid medium plates (Medium 63-F for LA8 and Medium 63-E for JM109) and incubated at 37°C overnight (≈16 h). The presence of 500 and 50 colonies using the 1:100 and 1:1000 diluents, respectively, corresponds to the required working concentration of 5 X 10^5 CFUs/ml. For each strain, the assay was run in duplicate.

MIC values were not calculated whenever a pellet of 2 mm or greater was observed in the growth control wells, or if the sterility control was turbid. The MIC value for MSI-78 was taken to be the lowest concentration of AMP that inhibited visible growth of the bacterial strain, as defined in Wiegand et al. [83].

3. Results

This section presents the results gained from the novel approach of characterizing peptide-membrane interactions of AMPs in intact *E.coli*. It begins with a discussion of the results of ^{2}H NMR studies of the K1060 strain – composed of labeled unsaturated chains (deuterated oleic acid) – in the absence and presence of the peptide MSI-78. These initial experiments used the K1060 strain because of its commercial availability at that time. However, unlike strains used in the past (e.g. Davis et al., [80]) the K1060 strain is only unable to synthesize unsaturated fatty acids. This means only selective ^{2}H labeling of the unsaturated chains is possible via incorporation of ^{2}H-labelled oleic acid into the growth media. This is followed by a discussion of the experiments done in order determine the optimal protocols to use for ^{2}H NMR studies of LA8, which is the novel strain with labeled saturated chains (deuterated palmitic acid). ^{2}H NMR studies on intact cells with saturated chains deuterated would facilitate better comparison with model membrane studies, which customarily have used deuterated saturated chains. This section also discusses the experiments done – cell counts, MTT assay and MIC assay – to characterize the LA8 strain. Finally, this section ends with a discussion of the results of the ^{2}H NMR studies of LA8 treated with MSI-78.

3.1 K1060 cultured using glucose

Given the availability of the K1060 strain (at the CGSC), it was decided to use this strain first to test the feasibility of ^{2}H NMR studies of entire bacteria in the presence of AMPs.

^{2}H NMR spectra were recorded for cells (labeled with deuterated oleic acid) cultured in Medium 63-C (glucose as carbon source) and harvested in the stationary phase. Figure 9 shows a series of spectra acquired at 37°C every 6 h, such that the first scan starts ≈2.5 h after the initial harvesting of bacteria. These spectra display monotonically increasing intensity as we approach the lower splittings (below ±15 kHz). Unlike multilamellar vesicles prepared using palmitoyl-2-oleoyl-sn-glycerol-3-phosphocholine (POPC) deuterated at the cis double bond of oleic acid, it was not possible to resolve doublets with splittings of approximately ±12 kHz, corresponding to the fluid C-10 deuterons of the double bond [84]. The spectra also have a sharp, central peak with a width of <1 kHz, which arises from naturally occurring deuterated water [71]. As time progresses, there are no visible changes in the spectra, indicating few changes to the lipid acyl chain order.

3.2 K1060 cultured using casamino acids

The next step was to investigate potential ways to increase the signal-to-noise ratio of the K1060 sample. Kongings et al., [64] studied the radio- and thermo-sensitivity of the K1060 strain. They cultured their bacteria in a minimal medium that used casamino acids as the carbon source instead of glucose. As such, a sample of K1060 strain was also cultured in medium containing casamino acids (Medium 63-D) in order to determine the effects the carbon source has on ^{2}H NMR spectra of the labeled oleyl

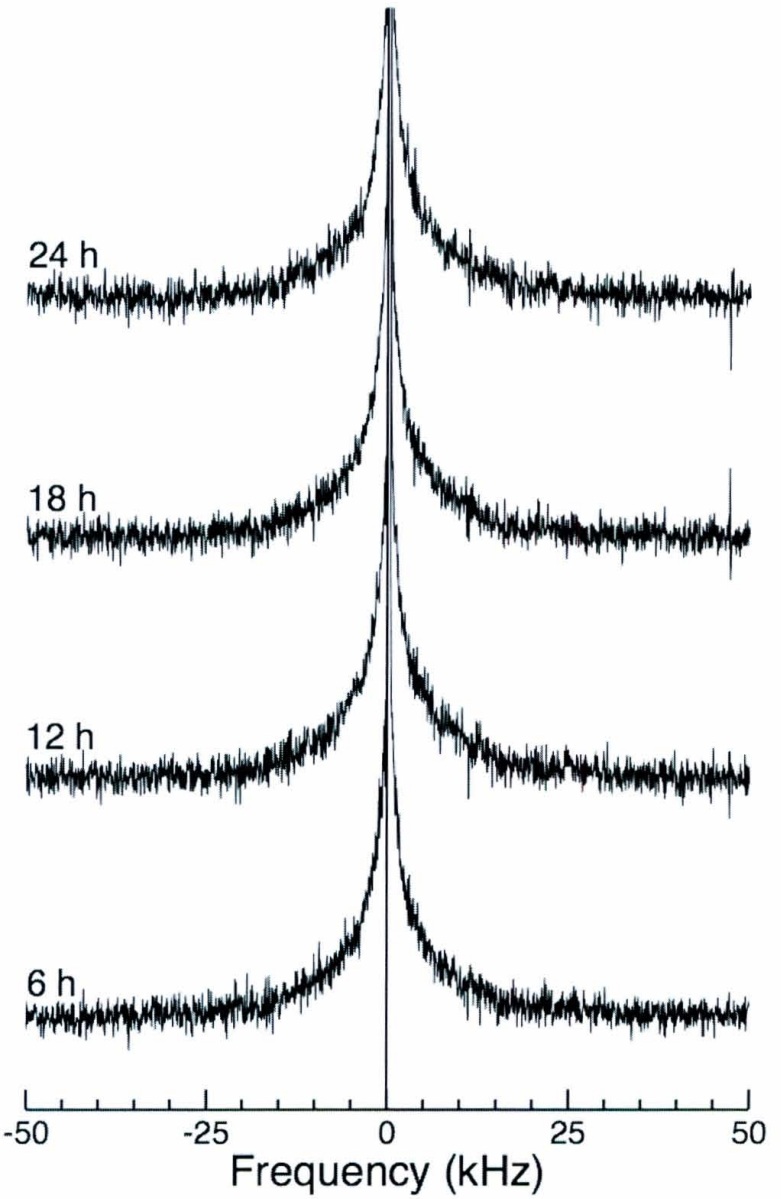

Figure 9. Solid-state ^{2}H NMR spectra of membrane-deuterated K1060 bacteria, showing the evolution of the NMR spectra over time. The bacterial samples were grown in media supplemented with glucose. Experiments were performed at 37°C and each spectrum represents 24000 scans.

chain. Using Medium 63-D, it was expected that deuterated oleic acid would constitute 72% of the fatty acids in the membrane [85].

Figure 10 compares the spectra acquired for the K1060 strain using the same growth protocol (Section 2.3) but different carbon sources: casamino acids and glucose. Both spectra were acquired at 37°C over a period of 12 h, with the first scan starting ≈2.5 h after the initial harvesting of bacteria. Both spectra display increased intensity at the lower splittings and decreased intensity at the higher splittings. However, the casamino acid spectrum is characterized by more prominent spectral edges at approximately ±15 kHz and ±7.5 kHz. The spectral peaks for the casamino acid sample are better resolved than those of the glucose sample; the casamino acid spectrum has a doublet arising from the C-10 deuterons of the double bond (approximately at ±2 kHz), which is missing in the glucose spectrum. Both spectra have a sharp central peak corresponding to naturally occurring deuterated water [71].

3.3 ^{2}H NMR studies of K1060 treated with MSI-78

Next ^{2}H spectra were acquired for K1060 cells (labeled with deuterated oleic acid) treated with the AMP, MSI-78. For these initial studies, the peptide was mixed in using vortexing, and thus control scans were also acquired with cells subjected to vortexing without the addition of AMP. Figure 11 shows ^{2}H NMR spectra of K1060 cultured in Medium 63-D and treated with varying concentrations of the antimicrobial peptide

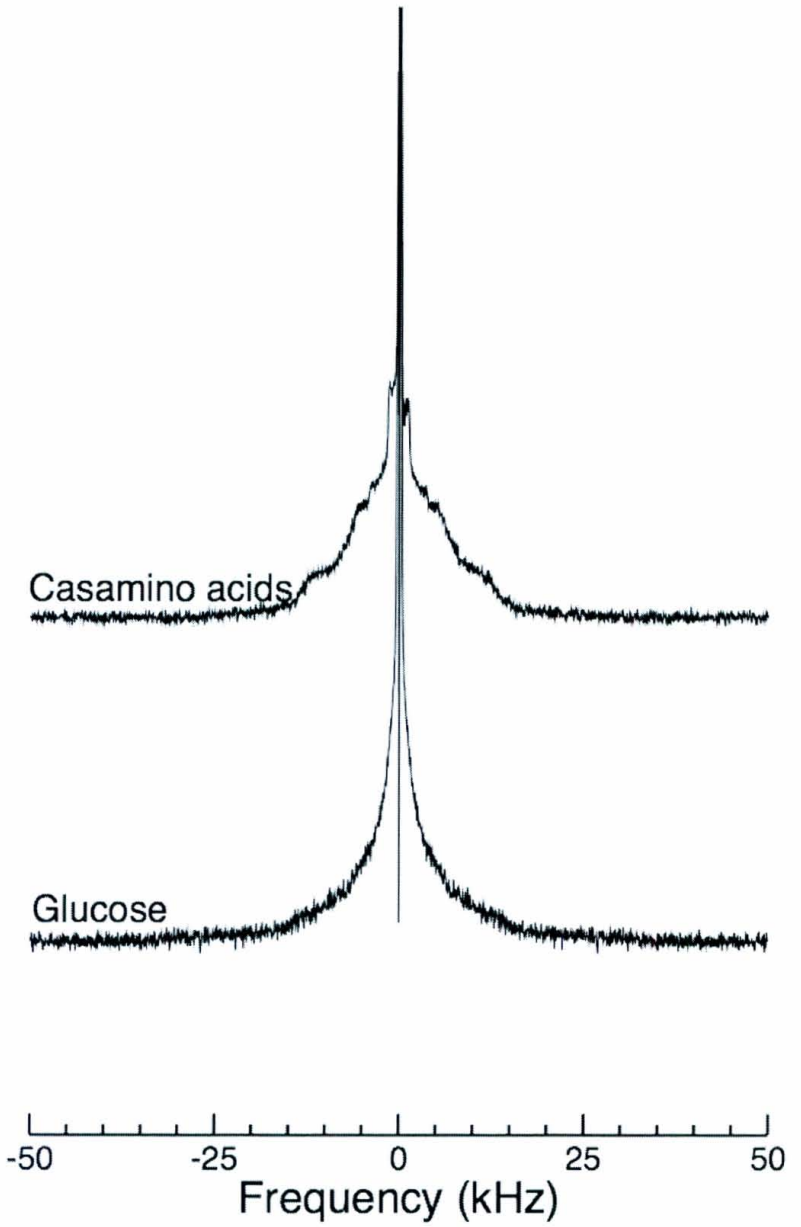

Figure 10. Solid-state ^{2}H NMR spectra of membrane-deuterated K1060 bacteria, showing the effects of different carbon sources in the growth media. Experiments were performed at 37°C and each spectrum represents 48000 scans.

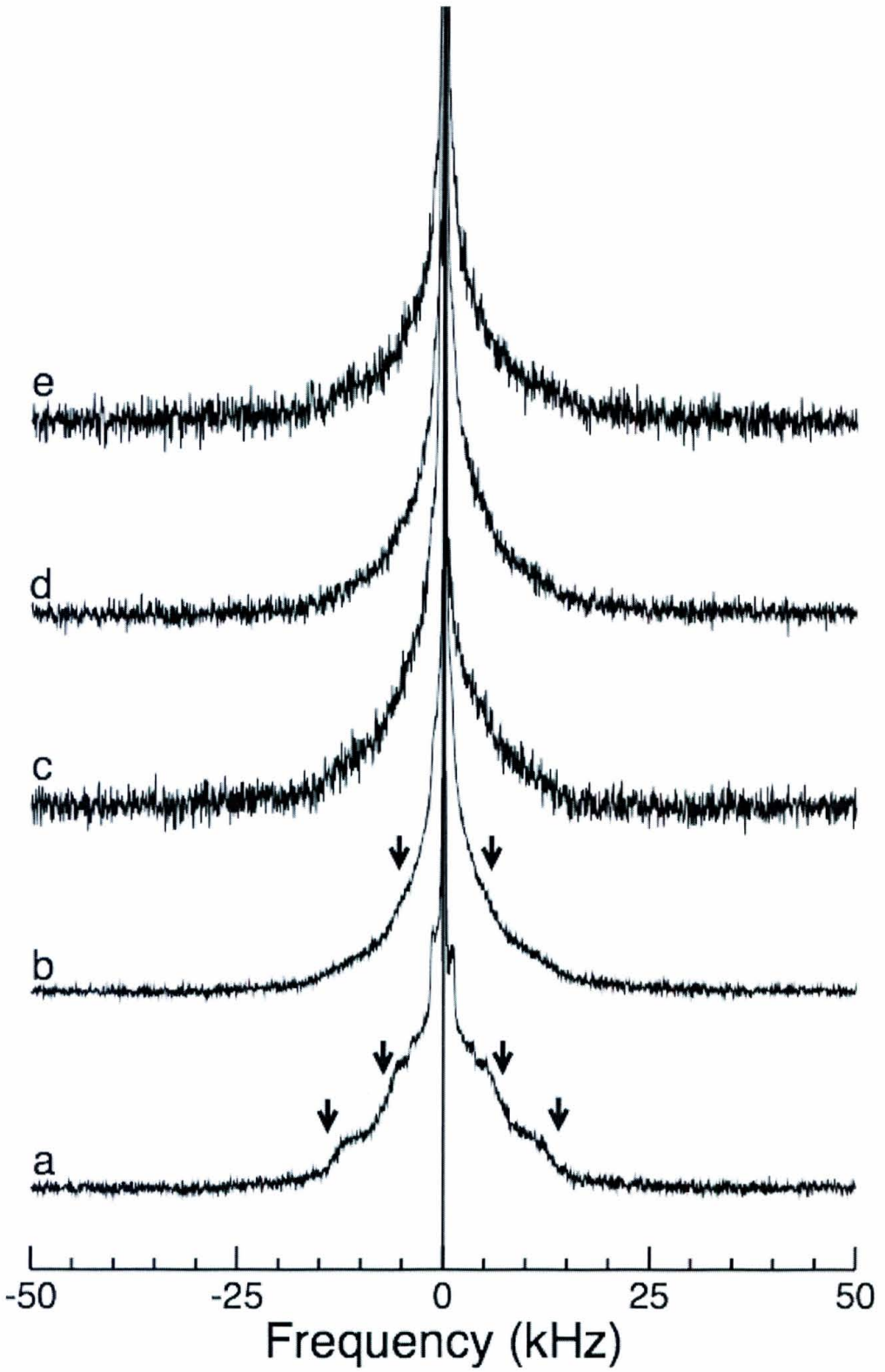
e
d
c
b
a
-50
-25
0
25
50
Frequency (kHz)

Figure 11. Solid-state ^{2}H NMR spectra of membrane-deuterated K1060 bacteria processed under different conditions. Experiments were performed at 37°C. (a) ^{2}H NMR spectrum of K1060 averaged over 48000 scans. Arrows correspond to spectral edges at approximately ±12 kHz and ±7.5 kHz. (b) ^{2}H NMR spectrum of K1060 subject to vortexing averaged over 152000 scans. Arrows correspond to spectral edges at approximately ±5 kHz. (c) ^{2}H NMR spectrum of K1060 in the presence of 10% w/w of MSI-78 (weight MSI-78 / dry weight bacteria x 100) (trial 1). The sample was subject to vortexing and averaged over 64000 scans. (d) ^{2}H NMR spectrum of K1060 in the presence of 10% w/w of MSI-78 (trial 2). The sample was subject to vortexing and averaged over 144000 scans. (e) ^{2}H NMR spectrum of K1060 in the presence of 20% w/w of MSI-78. The sample was subject to vortexing and averaged over 172000 scans.

MSI-78. Note that, as indicated in the figure legend, the spectra in Figure 11 were acquired with different numbers of scans, which led to the observed differences in signal-to-noise. All peptide concentrations are expressed as percentage of peptide weight over dry cell weight and all spectra were collected at 37°C. Treatment with MSI-78 (Figure 11c, 11d and 11e) resulted in an increase in intensity at smaller splittings with a subsequent decrease at larger splittings, indicating an increase in disorder of oleyl chains in the membrane. Vortexing (Figure 11b) had similar effects on the spectra but the effect appears to be greater in the presence of peptide. The ^{2}H NMR spectrum of the vortexed sample lacks the spectral edge seen at approximately ±15 kHz – seen in the peptide free non-vortexed sample – but still retains the spectral edge at the narrower splitting. However, the quadrupole splitting corresponding to this spectral edge is found at a lower frequency (approximately ±5 kHz) than for the peptide free non-vortexed sample (approximately ±7.5 kHz). The ^{2}H NMR spectra of the samples with peptide displayed no obvious spectral edges, possibly indicating a decrease in the orientational order of oleyl chains in all membrane fractions. However, the signal-to-noise ratios in these samples were low and it is hard to draw definite conclusions regarding the presence or absence of specific spectral features. Only the 10% (w/w) sample was repeated given the limited availability of MSI-78.

To quantify the changes in the spectra that occur with time, it is possible to calculate first spectral moments (M_1), which are proportional to the average order parameter of the ^{2}H-labelled lipid acyl chains. Also calculated, were the second moment (M_2) and the

mean square width of the distribution of splittings (Δ_2). Figure 12 shows the dependence of M_1, M_2, and Δ_2 on peptide concentration for the spectra in Figure 8. Vortexing and treatment with 10% MSI-78 resulted in lower values of M_1 and M_2, with a more substantial decrease in the presence of peptide. With vortexing the M_1 is ≈12% lower when compared to the no-peptide sample; in the presence of 10% MSI-78 and vortexing, the M_1 is ≈21% lower. In the presence of 20% MSI-78 and vortexing, the effects on M_1 and M_2 were less, than compared to the sample treated with 10% MSI-78 and vortexing or vortexing by itself. The response of Δ_2 to vortexing in the presence and absence of MSI-78 is opposite that of M_1 and M_2, reflecting its sensitivity to spectral shape rather than simply width. Δ_2 for K1060 treated with 10% MSI-78 was very different for the two trials. This is surprising since Δ_2 is less sensitive to baseline imperfection because it depends on the ratio of M_2 to M_1^2. This suggests that the calculated moments must be interpreted cautiously in such featureless and noisy spectra.

3.4 Echo decay times of K1060

In addition to acquiring the spectra of the K1060 strain under different conditions, quadrupole echo decay times were also measured. The quadrupole echo decay time reflects the sum of the motions that affect the quadrupolar interactions experienced by the deuterons. Figure 13 shows the echo decay times of K1060 bacteria cultured and treated under different conditions. For the K1060 strain, the type of media that it is cultured in – glucose or casamino acids as the carbon source – has little effect on the

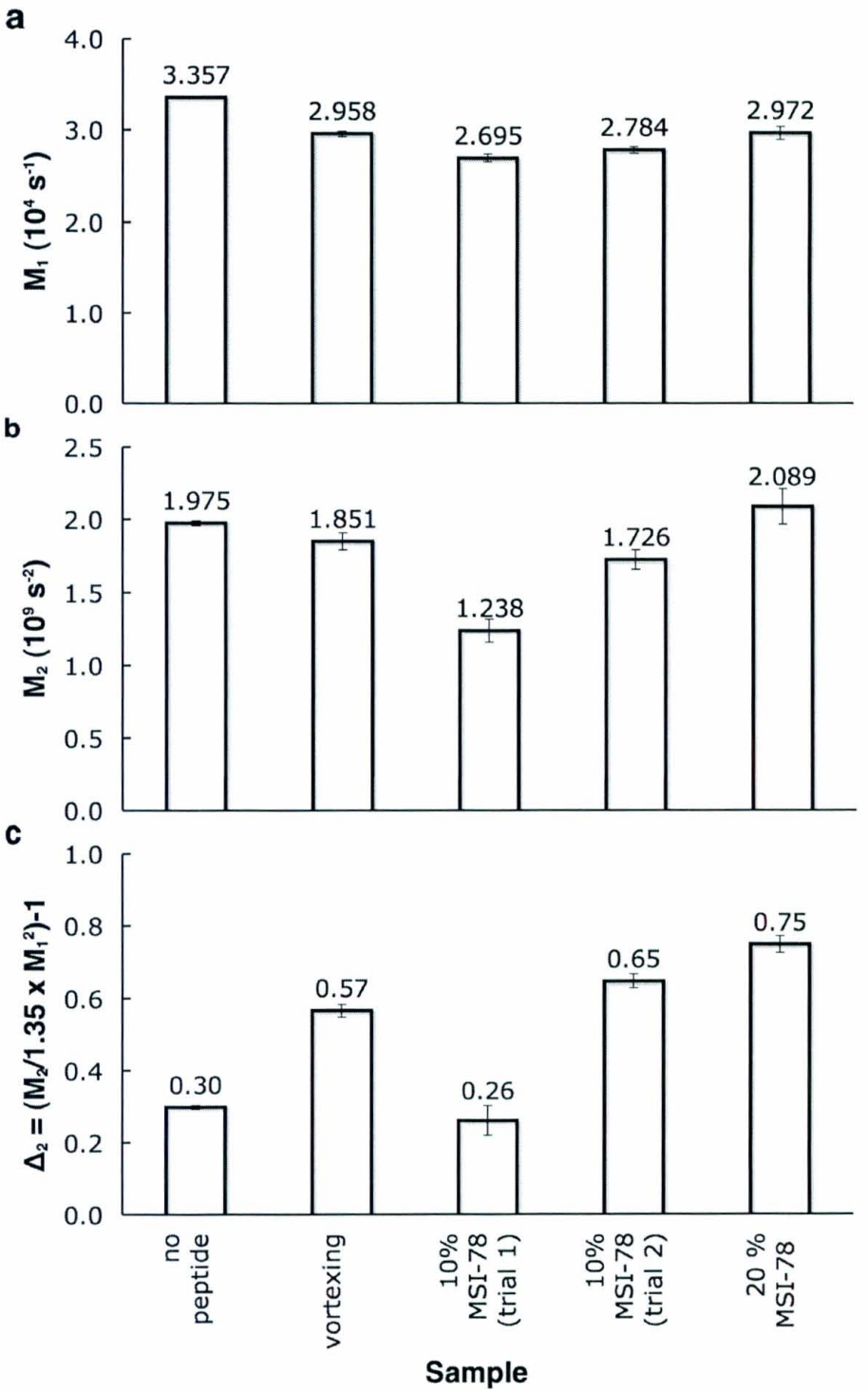
a
4.0
3.0
2.0
1.0
0.0
M1 (10^4 s^-1)
3.357
2.958
2.695
2.784
2.972
b
2.5
2.0
1.5
1.0
0.5
0.0
M2 (10^9 s^-2)
1.975
1.851
1.238
1.726
2.089
c
1.0
0.8
0.6
0.4
0.2
0.0
Δ2 = (M2/1.35 x M1^2)-1
0.30
0.57
0.26
0.65
0.75
no peptide
vortexing
10% MSI-78 (trial 1)
10% MSI-78 (trial 2)
20 % MSI-78
Sample

Figure 12. (a) First moment M1 , (b) second moment M2 , and (c) Δ2 of 2H-NMR spectra (Figure 11) for K1060 bacteria under different conditions: no peptide, refers to K1060 in the absence of MSI-78; vortexing, refers to K1060 that has been processed with buffer instead of MSI-78 (peptide control); 10% MSI-78, refers to a K1060 sample in the presence of 10% w/w of MSI-78 (weight MSI-78 / dry weight bacteria x 100); and 20% MSI-78, refers to a K1060 sample in the presence of 20% w/w of MSI-78. Error bars correspond to the uncertainty associated with extracting moments from a given spectrum.

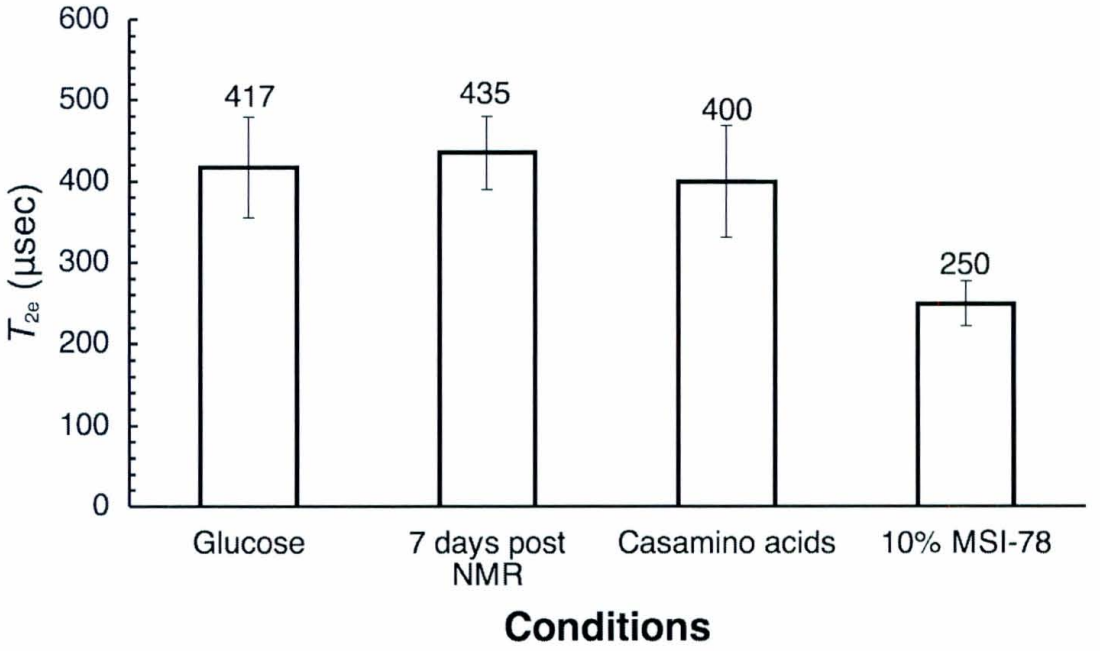

Figure 13. NMR quadrupolar echo decay time $|T_{2e}|$ at 37°C for membrane-deuterated K1060 bacteria under different conditions: Glucose, refers to K1060 grown in media supplemented with glucose; 7 days post NMR, is the decay time for the glucose sample 7 days after the initial experiment; Casamino acids, refers to K1060 grown in media supplemented with casamino acids; and 10% MSI-78, refers to a K1060 sample in the presence of 10% w/w of MSI-78 (weight MSI-78 / dry weight bacteria x 100). *Error bars* correspond to the uncertainty associated with calculating decay times.

decay time, which is approximately 400 μs. The treatment of K1060 with 10% MSI-78 results in a substantial decrease in $T_{2e,}$ which may reflect an increase in range of lipid chain reorientations.

3.5 Preparation of saturated chain labeled bacteria

Model membranes with deuterated saturated chains have been more extensively studied (e.g. [86] and [87]) than those with deuterons on the unsaturated chain. As such, it was concluded that conducting ^{2}H NMR studies on intact cells with saturated chains deuterated would facilitate comparison with model membrane studies. For ^{2}H NMR studies of entire bacteria, it was desirable to maximize the level of ^{2}H labeling in the membranes and minimize the ^{2}H background signal from elsewhere in the bacteria. To accomplish this, a novel strain of *E. coli* (termed LA8) was created that is unable to synthesize or metabolize fatty acids, allowing for selective ^{2}H labeling of the saturated chains of most phospholipids via incorporation of ^{2}H-labelled palmitic acid into the growth media [80]. The starting point for producing LA8 was the L8 strain of bacteria, which has a mutation that renders it unable to synthesize fatty acids [69]. Using the system of Datsenko and Wanner [75], genetic manipulations were introduced to the strain (refer to section 2.4). By replacing the *fadE* gene with a kanamycin resistance gene (*kan*) these bacteria lost the ability to metabolize fatty acids. Based on the similarity between the LA8 and L51 strains [80] and the growth protocol employed, it is expected 96% of the phosphatidylethanolamine (PE) – the major phospholipid in the

bacterial membrane [88] – to have a deuterated palmitic acid in the sn-1 position. Since palmitic acid is the major naturally occurring saturated fatty acid, deuterated palmitic acid is expected to be present in all other phospholipids as well [107].

3.6 ^{2}H NMR studies of LA8 in a high field spectrometer

Davis et al., [80] studied the effects of temperature on the cytoplasmic and outer membranes of *E. coli* by ^{2}H NMR, using a strain metabolically similar to LA8. However, they used a shorter recycling delay (i.e. more scans per second) and a longer pulse separation. In order to check for sensitivity of the observed signal to acquisition parameters, similar settings as those used by Davis et al. were tested when working with the LA8 strain. ^{2}H NMR studies were next performed using the higher field 9.4 T solid-state NMR spectrometer. Figure 14a shows a series of spectra acquired using acquisition parameters based on a shorter pulse recycling delay and longer pulse separation. Figure 14b is a spectrum obtained using a 500 ms recycling delay and 60 μs pulse separation. The increased pulse separation had little effect on the spectrum and it was similar to the spectrum in Figure 14a. All spectra still have a sharp central peak corresponding to deuterated water and show no visible changes with time. ^{2}H NMR studies of LA8 were also performed on the same 9.4 T solid-state NMR spectrometer using the following pulse parameters: a 900 ms recycling delay and a 30 μs pulse separation. The shorter pulse separation reduces the loss of signal due to echo decay. ^{2}H NMR spectra were recorded for cells cultured in Medium 63-B and harvested in the stationary phase.

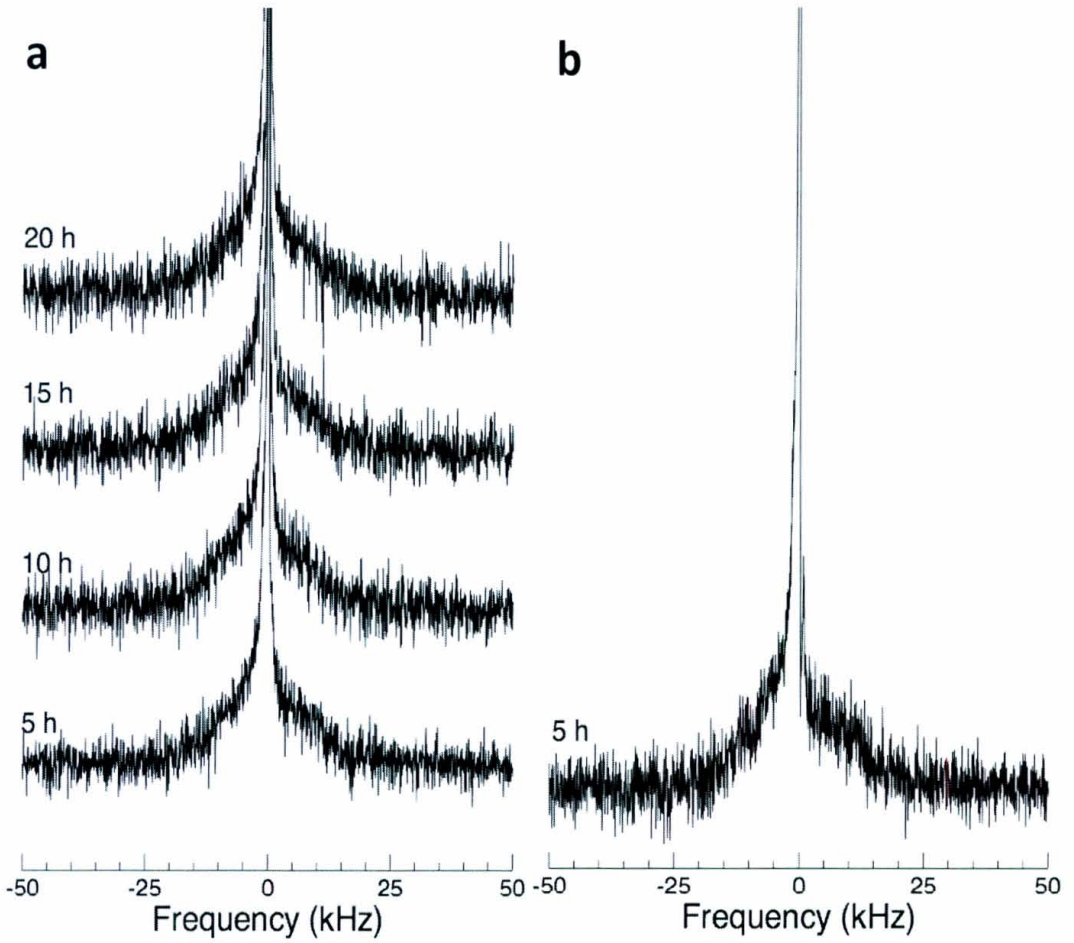

Figure 14. Solid-state ^{2}H NMR spectra of membrane-deuterated LA8 bacteria using a 9.4 Tesla solid-state NMR spectrometer at 37°C. Each spectrum represents 40000 scans. (a) ^{2}H NMR spectra showing the evolution of the NMR spectra over time using a 500 ms recycling delay and 40 μs pulse separation. (b) ^{2}H NMR spectrum obtained using a 500 ms recycling delay and 60 μs pulse separation.

Figure 15a shows a series of spectra acquired at 37°C every 2 h, such that the first scan starts ≈2.5 h after the initial harvesting of bacteria. These spectra display increased intensity at the lower splittings relative to the higher splittings. Spectral edges are somewhat noticeable at approximately ±12 kHz. This is more obvious in Figure 15b, which shows spectra with better signal-to-noise ratios collected over a period of 8 h and 18 h, respectively. All of the spectra still display a sharp, central peak, which arises from naturally occurring deuterated water [80]. As time progresses, there are no visible changes in the spectra, indicating few changes to the lipid acyl chain order.

3.7 Optimization of bacterial preparation protocols

In order to test the effects of growth phase on the ^{2}H NMR spectra, LA8 was cultured in Medium 63-B and harvested at an A_{600} = 1.191. This corresponds to the later stage of the exponential growth phase. Figure 16a shows a series of spectra acquired at 37°C every 2 h, such that the first scan starts ≈2.5 h after the initial harvesting of bacteria. The spectra display more intensity at the lower splittings relative to the higher splittings. The spectra display spectral edges at approximately ±12 kHz which disappear with time. As time progresses, there is a decrease in the intensity at the higher splittings and an increase in intensity at the lower splittings. This results in a loss of the spectral edges at approximately ±12 kHz and indicates an increase in the lipid acyl chain disorder over time. Figure 16b includes spectra collected over a period of 8 h and 16 h, respectively. When comparing ^{2}H NMR spectra of LA8 from the stationary phase (Figure 15b) and the exponential phase (Figure 16b), cells harvested in the exponential phase

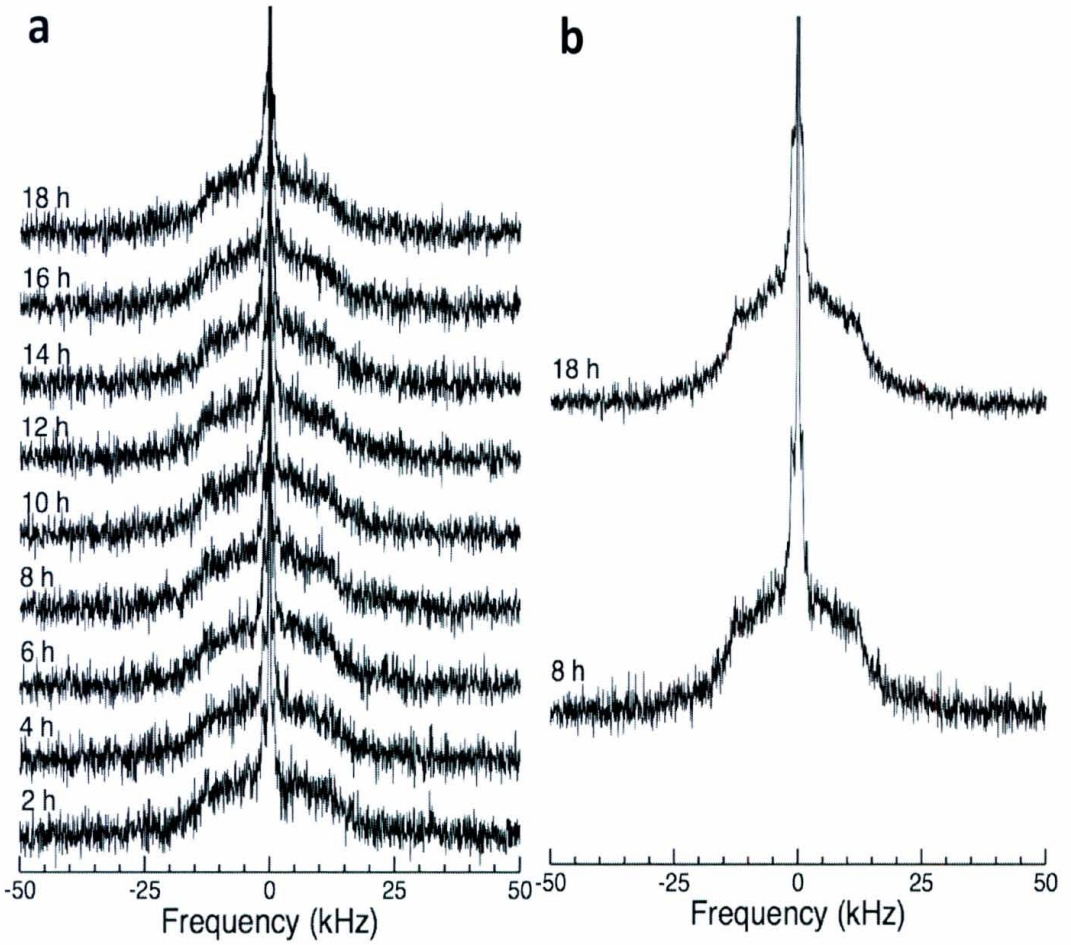

Figure 15. Solid-state ^{2}H NMR spectra of membrane-deuterated LA8 bacteria using a 9.4 Tesla solid-state NMR spectrometer at 37°C with a 900 ms recycling delay and 30 µs pulse separation. (a) ^{2}H NMR spectra showing the evolution of the NMR spectra over time. Each spectrum represents 8000 scans. (b) ^{2}H NMR spectra of LA8 averaged over 32000 scans (8 h) and 72000 scans (18 h)

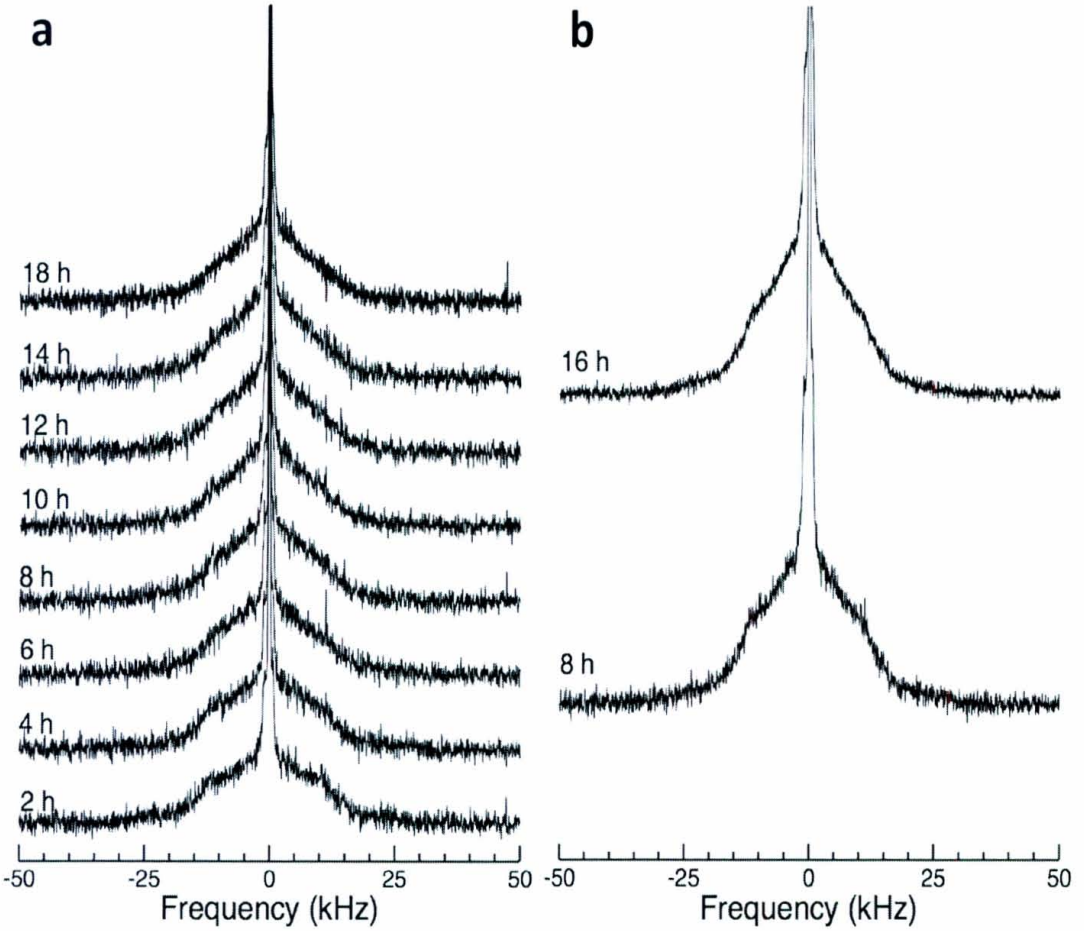

Figure 16. Solid-state ^{2}H NMR spectra of membrane-deuterated LA8 bacteria obtained using a shorter culture time and grown to A_{600} = 1.191. (a) ^{2}H NMR spectra showing the evolution of the NMR spectra over time. Experiments were performed at 37°C and each spectrum represents 8000 scans. The 16 h spectrum was omitted due to a missed scan (b) ^{2}H NMR spectra of LA8 averaged over 32000 scans (8 h) and 64000 scans (16 h). Experiments were performed at 37°C.

show much better signal-to-noise ratios. All of the spectra still display a sharp, central peak, which arises from naturally occurring deuterated water [80].

Since a shorter growth protocol gave ^{2}H NMR spectra with improved signal-to-noise ratio, it was thought that a shorter processing time (accomplished by doing only one wash) might have the same effect and this possibility was tested. The washing step removes any free labeled palmitic acid that was not incorporated into the membrane. Figure 17 shows a series of spectra acquired at 37°C every 2 h, such that the first scan starts ≈2 h (only one wash) after the initial harvesting of bacteria. This sample of LA8 was cultured in Medium 63-B and harvested it at an A_{600} = 1.237 (late exponential phase). The spectra display increased intensity at the lower splittings relative to the higher splittings. As time progresses, there is a decrease in the intensity at the larger splittings and an increase in intensity at the lower splittings, indicating an increase in disorder of the lipid acyl chain as before. All spectra display a prominent spectral edge at approximately ±12 kHz. When compared to similar spectra obtained using two washes (Figure 16a), the above spectra show improved signal-to-noise ratios and the spectral edges are better resolved.

3.8 LA8 growth curve

Based on the previous results, harvesting bacteria with only one wash and isolating them in the exponential phase produced spectra with the best signal-to-noise ratio. As such, it was important to measure the growth curve for the LA8 bacteria in order to more accurately determine the exponential growth phase (also known as the logarithmic phase). This growth curve is shown in Figure 18. Based on the growth curve,

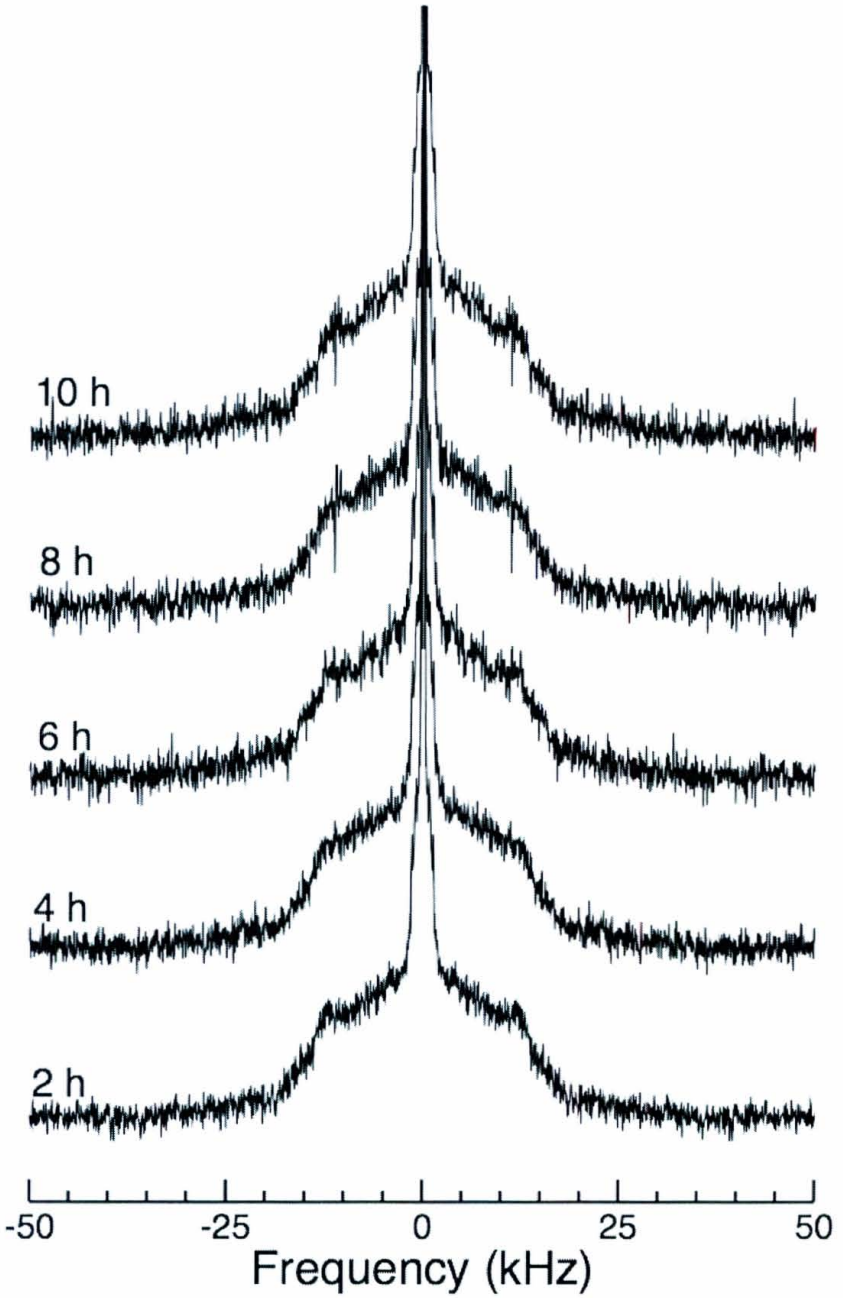

Figure 17. Solid-state ^{2}H NMR spectra of membrane-deuterated LA8 bacteria, showing the evolution of the NMR spectra over time. Samples were grown to an A_{600} = 1.237 and washed only once. Experiments were performed at 37°C and each spectrum represents 8000 scans.

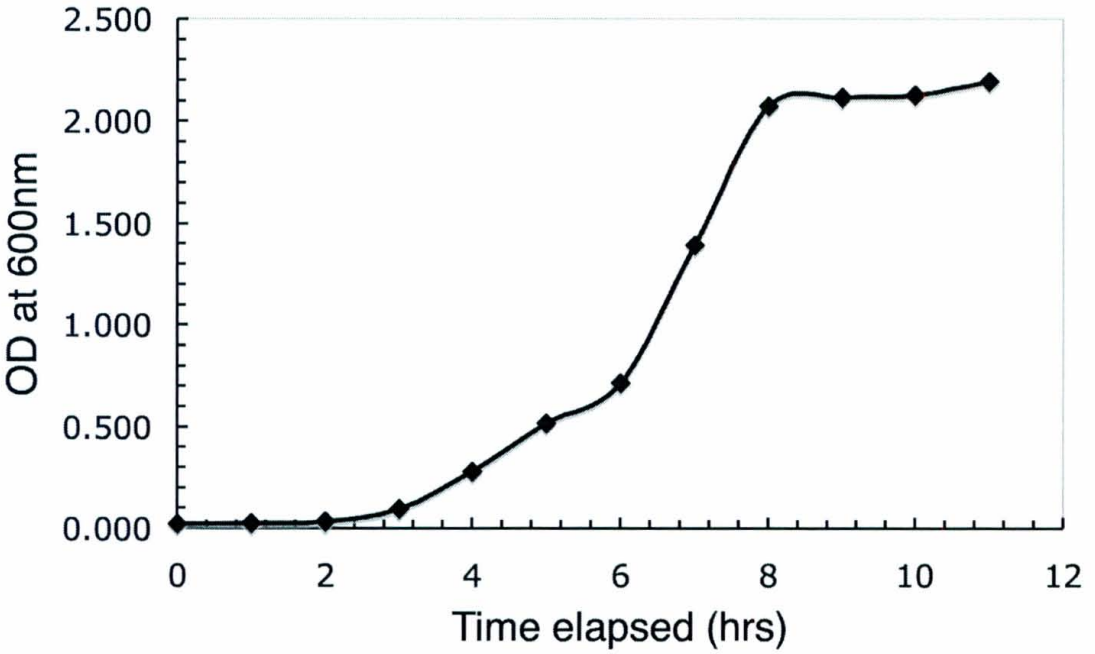

Figure 18. Growth of LA8 bacteria as measured by absorbance at 600nm |OD_{600}|. Cells were inoculated from an overnight culture at time zero and then grown at 37°C at 170 rpm in minimal media supplemented with oleic and palmitic acid.

the mid-log phase of growth occurs ≈6-7 hours after inoculation of the overnight culture into fresh media. It was expected that cells isolated in the mid-log phase would produce the best spectra; at this stage there is a higher rate of membrane biogenesis, the media is still rich in nutrients and there is very little cell lysis [90].

3.9 ^{2}H NMR studies of LA8 using new protocols

^{2}H NMR spectra were acquired for the ^{2}H membrane-labeled LA8 bacteria harvested in the mid-log phase (A_{600} = 0.6 – 1.0) and washed only once. Figure 19a shows a series of spectra acquired at 37°C every 2 hours, such that the first scan starts 2 hours after the initial harvesting of the log-phase bacteria. Figure 19b isolates the spectrum at two hours and illustrates some of the spectral features. These spectra at 37°C display a prominent shoulder near ±12 kHz, resembling spectra from lipid liposomes just above their gel-to-liquid crystalline transition temperature (e.g. [91] [80]). The shoulder at approximately ±12 kHz (indicated by arrows labeled "p" in Figure 19b) arises from deuterons on the motionally constrained region of the deuterated palmitate chains near the headgroup, and corresponds to the plateau region of the orientational order parameter profile [81, 92]. The quadrupole splittings decrease with proximity of the deuterated chain segment to the bilayer centre, with those groups near the center having a smaller splitting. The doublet arising from methyl groups at the deuterated chain ends is labeled by "m" in Figure 19b. The spectra have a sharp, central peak with a width <1 kHz, which arises from naturally occurring deuterated water [80]. This feature is labeled "w" in Figure 19b. As time progresses, there is a decrease in the intensity at the larger splittings and an increase in intensity at the lower

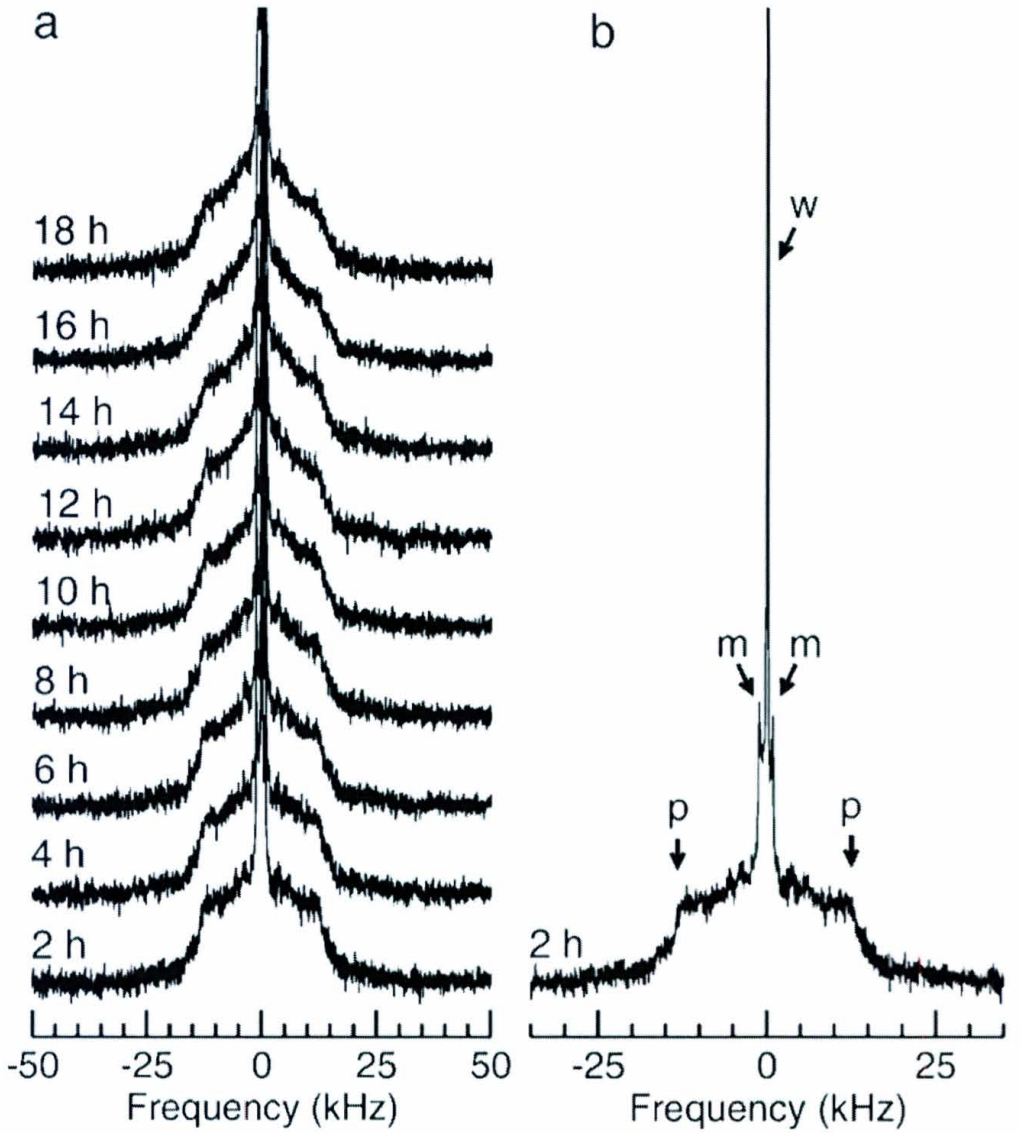

Figure 19. (a) Solid-state ^{2}H NMR spectra of membrane-deuterated LA8 bacteria, showing the evolution of the NMR spectra over time. Experiments were performed at 37°C and each spectrum represents 8000 scans. (b) Isolated trace of the 2 h spectrum with arrows to indicate the water peak (w), palmitate methyl deuteron doublet (m), and the prominent edges (p) corresponding to the quadrupole splitting deuterons near the headgroup, and thus most motionally-constrained, end of the acyl chain. This feature is typically associated with the plateau region of the orientational order parameter profile.

splittings, indicating an increase in the lipid acyl chain disorder over time.

3.10 Time-dependent quantitative NMR studies of LA8

To quantify the changes in the spectra (Figure 19a) that occur with time, spectra were analyzed by calculating the first moments (M_1), the second moments (M_2) and the mean square width of the distribution of splittings (Δ_2). The first moment M_1 decreases slowly with time (Figure 20a), reflecting an overall decrease in the average order parameter due to increased amplitude of motions of the acyl chains in the bacterial membrane. Over the course of 18 hours, M_1 values for the untreated bacteria decrease from an initial value of $\approx 5 \times 10^4$ s^{-1} to $\approx 4.5 \times 10^4$ s^{-1}. The bacterial membranes are only slightly less ordered than model lipid membranes – such as multilamellar vesicles composed of DPPC-d_{62} – and typically exhibit M_1 values of $\approx 5 \times 10^4$ s^{-1}, just above their transition temperature [93][94]. Figure 20b shows corresponding values of the second spectral moment M_2. Because of the differences in how intensity at a given splitting contributes to the first and second moments, an appropriate comparison of these moments can be sensitive to spectral shape. This comparison is provided by Δ_2, the relative mean square width of the distribution of orientational order parameters. In Figure 20c, Δ_2 increases as the spectral shape changes from having more prominent shoulders near ±12 kHz to having less prominent shoulders and relatively more intensity at smaller splittings.

In preparing the bacteria for NMR, the cells are washed and resuspended in buffer. Thus, the slow reduction in M_1 and corresponding changes in M_2 and Δ_2 over

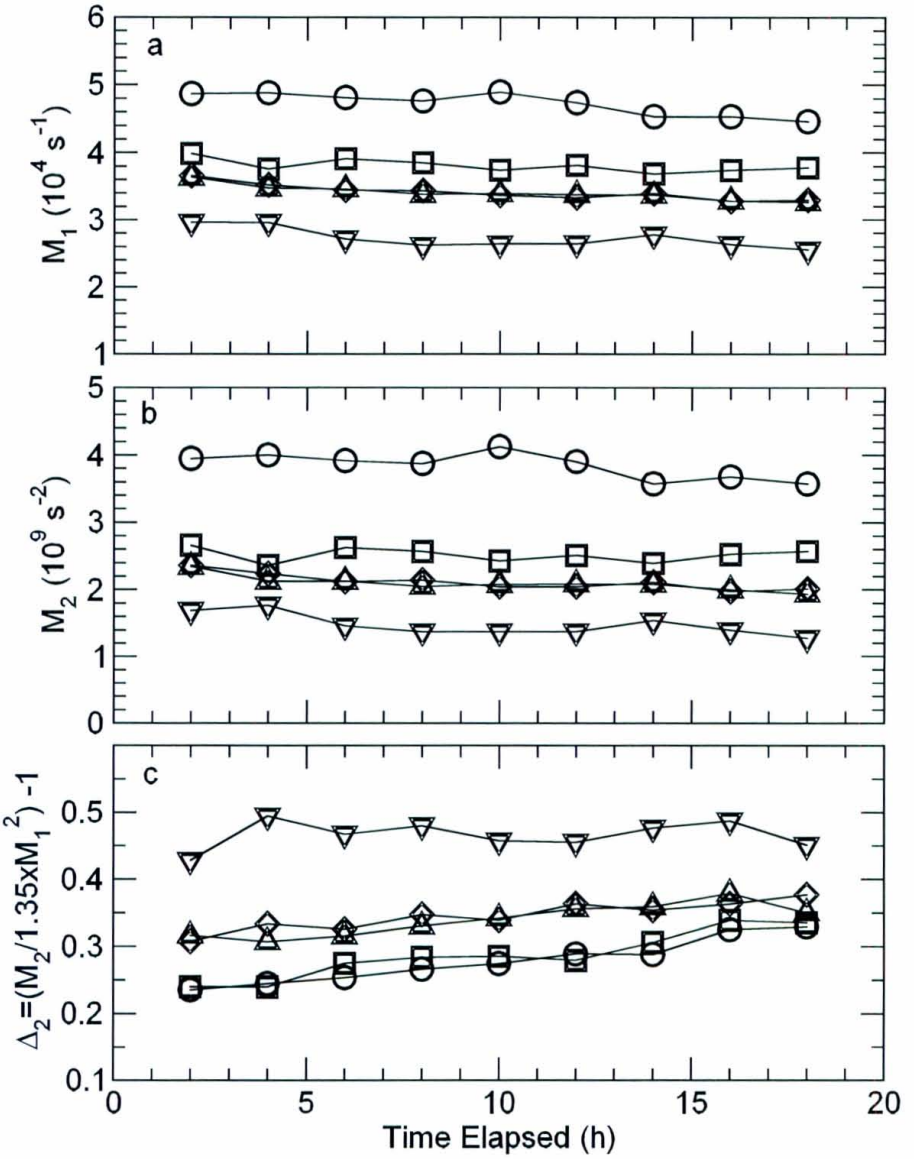

Figure 20. (a) First moment M_1 , (b) second moment M_2 , and (c) Δ_2 of ^{2}H-NMR spectra from membrane-deuterated LA8 bacteria as a function of time in the presence of increasing concentrations of MSI-78. Time = 0 h refers to the moment the NMR study began following sample processing, i.e. two hours after the cells are initially harvested. Concentrations of MSI-78 (w/w) are (circle) 0% peptide, (square) 10% peptide, (diamond) 20% peptide, (triangle up) 30% peptide, and (triangle down) 60% peptide.

time is likely related to the absence of nutrients available to the cells while they are in the NMR spectrometer.

3.11 Cell viability (MTT and plate counts)

To relate the measured ^2H NMR spectral results with biological function, cell viability assays were carried out under conditions identical to those used in the NMR experiments (Figures 21 & 22). The plate count assay (Figure 21a and 21b) indicated that the initial washing of the bacteria led to a loss of ≈45% of the viable cells on average. Six hours after washing (i.e. after the first 3 spectra shown in Figure 19a), 76% of these cells were still capable of forming colonies, on average. After 12 and 18 hours, approximately 50% of the cells that went into the NMR spectrometer retained their capability to form colonies. The rate of loss of colony-forming units was quite high compared to the rate of decrease in M_1. This suggests that cell death may not be accompanied by large changes in M_1, or that a substantial population of bacteria do not necessarily die during the NMR experiment but do lose their ability to form colonies within the time span of this assay.

In contrast to the plate count assay, the MTT assay (Figure 22a and 22b) indicates that the initial washing of the bacteria leads to a loss of ≈15% of the metabolically active cells on average. For all time intervals after washing (6 h, 12 h, 18 h and 24 h), 64% of the original unprocessed culture is still metabolically active on average (i.e. ≈75% of the cells remain metabolically active post-washing). These measured values correlate more readily with the slow decrease in M_1 and M_2 seen in Figures 20a and 20b. The cell viability observed via the MTT assay does not coincide with the plate count

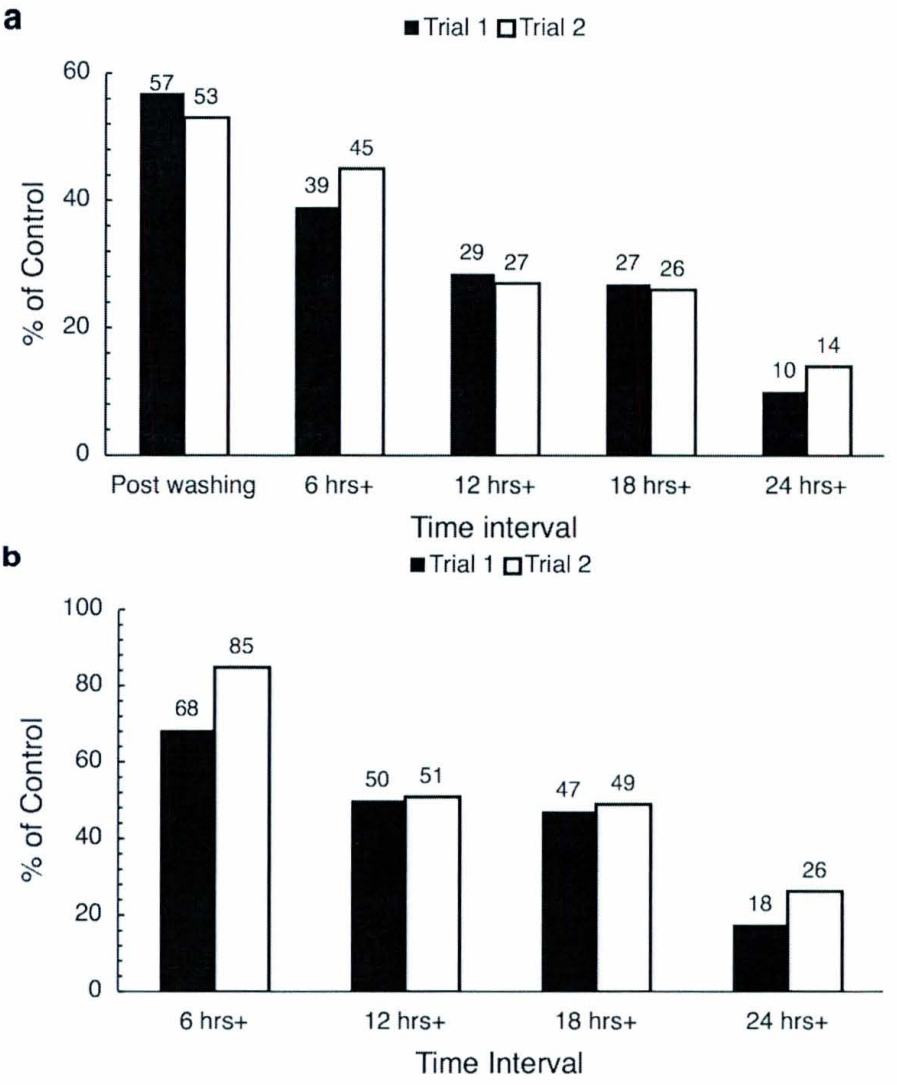

Figure 21. Plate counts for cells plated immediately after processing and before the NMR experiments, as well as for cells held under conditions identical to NMR and plated after 6, 12, 18 and 24 hours. (a) Cell viability expressed as a percentage relative to unprocessed cells plated before washing. (b) Cell viability expressed as a percentage relative to processed cells plated after washing. The black and white bars represent two separate experiments performed at each time point.

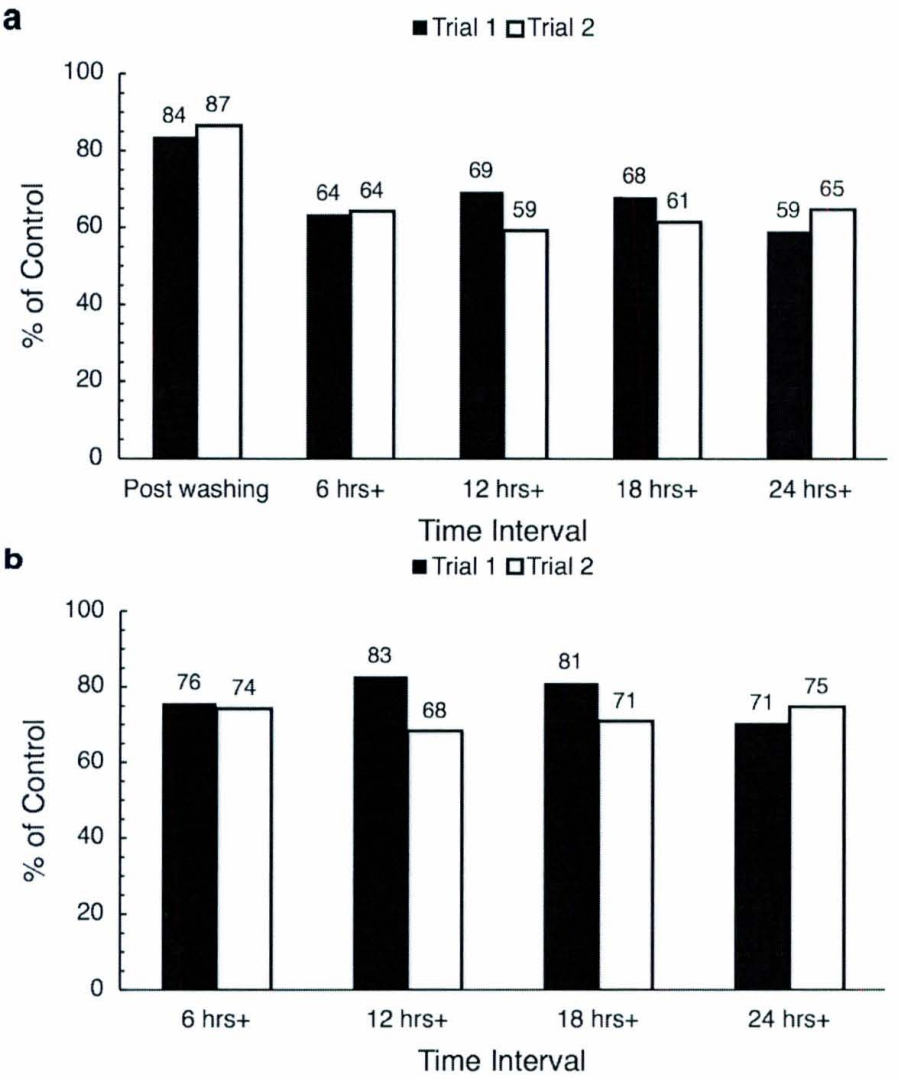

Figure 22. Absorbance at A_{550} of formazan crystals produced by *E. coli* cells immediately after processing and before the NMR experiments, as well as for cells held under conditions identical to NMR and measured after 6, 12, 18 and 24 hours. (a) Cell viability expressed as a percentage relative to unprocessed cells measured before washing. (b) Cell viability expressed as a percentage relative to processed cells measured after washing. The black and white bars represent two separate experiments performed at each time point.

assay. This suggests that, although the cells may lose the ability to form colonies (as seen in Figure 21), it might not correspond to cell death (as seen in Figure 22).

3.12 Determination of minimal inhibitory concentration (MIC) for MSI-78

Since a novel strain of *E. coli* (LA8) was created, it is important to characterize the antimicrobial activity of MSI-78 against this strain. This can be used to determine the expected effects that the various concentrations of MSI-78 would have on the cells. The antimicrobial activity can be assessed by a minimal inhibitory concentration (MIC) assay, which determines the lowest concentration of a peptide required to inhibit growth of bacteria [83]. The MIC values of MSI-78 were determined for the strains LA8 and JM109 (wild-type *E. coli*). Based on MIC values, MSI-78 was four times more active against the LA8 strain than against the wild-type JM109 strain (Table 4, Figure 23), which suggests the physiology of the LA8 could be quite different from the corresponding wild-type.

Peptide (Strain)		1	2	3	4	5	6	7	8	9	10	11	12
MSI-78	trial 1	X	X	X	X	X	√	√	√	√	√	GC	SC
(LA8)	trial 2	X	X	X	X	X	√	√	√	√	√	GC	SC
MSI-78	trial 1	X	X	X	√	√	√	√	√	√	√	GC	SC
(JM109)	trial 2	X	X	X	√	√	√	√	√	√	√	GC	SC

Figure 23. Graphical representation of the portion of a 96-well plate used for the MIC assay (Section 2.10). Note that an "X" represents no growth and a "√ " represents normal growth. GC represents the growth control and SC represents sterility control. Columns 1 through 10 represent a doubling dilution series of the peptide MSI-78, with column 1 at 100 μg/ml and column 10 at 0.195 μg/ml.

Table 4. Results of antimicrobial susceptibility testing; MSI-78 minimal inhibitory concentration (MIC) values for mutant (LA8) and wild type (JM109) species of *Escherichia coli.*

	MSI-78 (μg/ml)[1]
LA8	6.25 (± 3.13)
JM109	25.0 (± 12.5)

[1]MIC determination and solution conditions for the assay can be found in section 2.10.

3.13 Time-averaged ^{2}H NMR studies of LA8 treated with MSI-78

Figure 24a shows time-averaged ^{2}H-NMR spectra of ^{2}H membrane-labeled LA8 bacteria treated with varying concentrations of the antimicrobial peptide MSI-78. These spectra represent averages of the first 8 hours of data collection and thus show a better signal-to-noise ratio compared to the spectra displayed in Figure 19a (which represent 2 hour scans). Treatment with MSI-78 resulted in an increase of intensity at smaller splittings relative to larger splittings, indicating a decrease in average orientational order with increasing amounts of MSI-78. The quadrupole splitting corresponding to the spectral shoulder (arrows in Figure 24a) is found to decrease with increasing peptide concentration. The spectra may still reflect a shift in the relative populations of different membrane regions with varying levels of order, but, in contrast to the changes with time shown in Figure 18a, there is no fraction of the membrane for which orientational order is not diminished as peptide concentration increases. Figures 24b, 24c and 24d show the dependence of M_1, M_2, and Δ_2, respectively, on peptide concentration for the spectra in Figure 24a, plus those for two duplicate samples prepared with no peptide

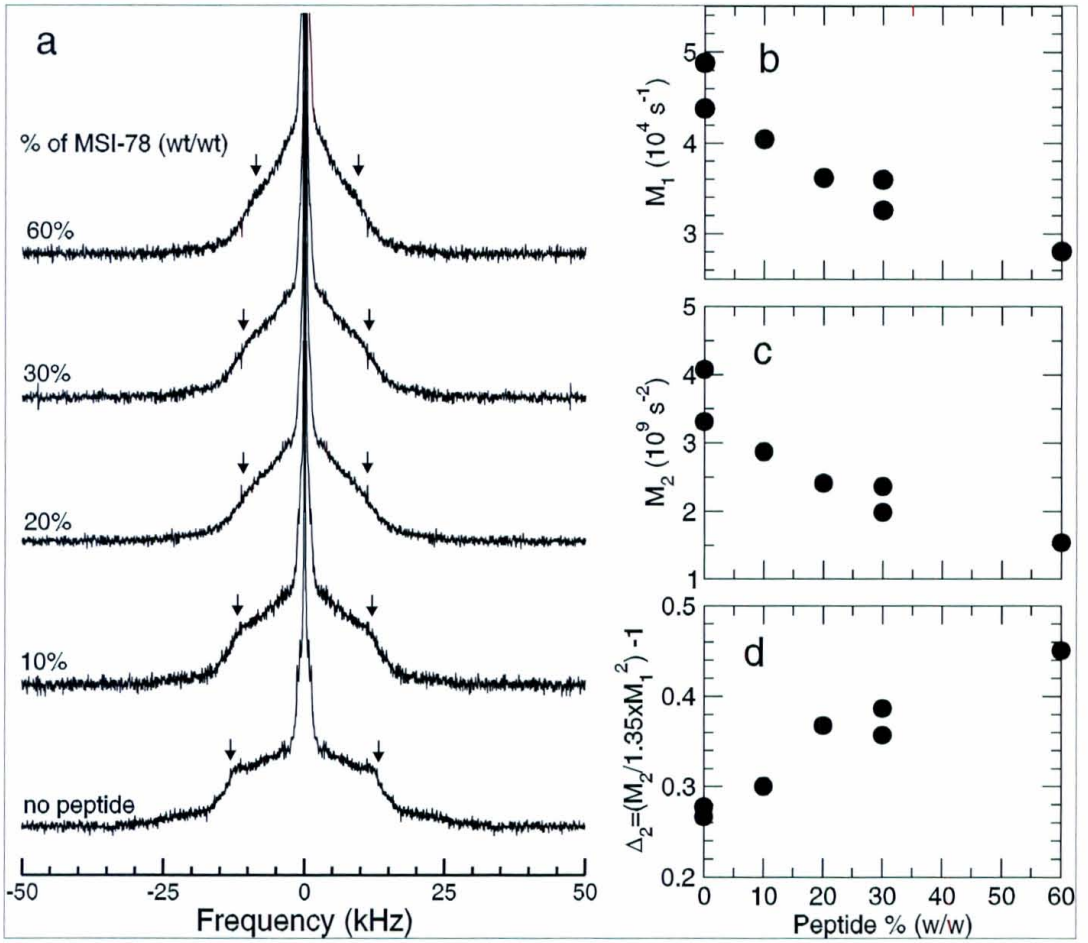

Figure 24. (a) Solid-state ^2H NMR spectra of membrane-deuterated LA8 bacteria with increasing concentrations of MSI-78. MSI-78 concentrations are quoted as weight MSI-78/dry weight bacteria × 100. NMR experiments were performed at 37°C and each spectrum represents 32000 scans. The right panel shows (b) the first moment M_1 , (c) second moment M_2 , and (d) Δ_2 versus peptide concentration for the spectra in panel (a) and the spectra of duplicate samples at peptide concentrations of 0% and 30%.

and 30% w/w MSI-78. These panels clearly show the effect of the peptide on both the average orientational order along the deuterated chain (M_1) and the distribution of intensity across the spectrum (Δ_2).

As with the untreated cells, the shape of the spectra for the MSI-78-treated bacteria were quantified in terms of M_1, M_2 and Δ_2 , calculated for each 2 hours of NMR data acquisition and plotted in Figures 20a, 20b, and 20c. For the treated bacteria, the slow changes in M_1, M_2 and Δ_2 over time occurred at approximately the same rate as the untreated bacteria. However, each M_1, M_2 or Δ_2 vs. time curve was displaced in response to MSI-78 treatment, to an extent consistent with the peptide concentration. These dependencies are illustrated in Figures 24b, 24c, and 24d as well. In general, increasing concentrations of MSI-78 resulted in lower values of M_1 and M_2, although the values for 20% and 30% peptide w/w were similar. The response of Δ_2 to peptide concentration is opposite that of M_1 and M_2, reflecting its sensitivity to spectral shape rather than simply width. The reductions in M_1 with peptide treatment are substantial. For example, with 20% MSI-78 the initial M_1 is ≈20 % lower than for the untreated cells. The decrease in initial M_1 with increasing peptide concentration is also large when compared to the change in M_1, observed for all the samples over the 18-hour total experiment time. The results displayed in Figures 24b, 24c, and 24d for duplicate untreated and 30% peptide samples illustrate reproducibility, particularly for Δ_2 which, because it depends on the ratio of M_2 to M_1^2, is less sensitive to baseline imperfection. Control experiments with buffer (Medium 63) in place of AMP demonstrated that the

additional 15 minute re-suspension and treatment steps employed for the AMP-treated bacteria led to decreases in M_1 of less than 2.3%.

3.14 Echo decay of LA8

The effects of MSI-78 on bacterial membranes were also investigated by measuring the quadrupolar echo decay time (T_{2e}) of LA8 with varying peptide concentrations (Figure 25). It is interesting that the quadrupole echo decay times observed here (and summarized in Figure 25) are somewhat low compared to those normally seen in the liquid crystalline phase of model bilayers [95]. This may reflect a larger range of lipid chain reorientation in the more compositionally heterogeneous environment of the natural membrane. For most of the peptide concentrations used, the effect on T_{2e} is quite modest. However, for 60% MSI-78 w/w, there is a substantial drop in T_{2e}, perhaps indicating a loss of integrity of the membrane on a larger scale, and that the average angular range of lipid reorientation is increasing, as suggested by the observed decrease in average quadrupole splitting.

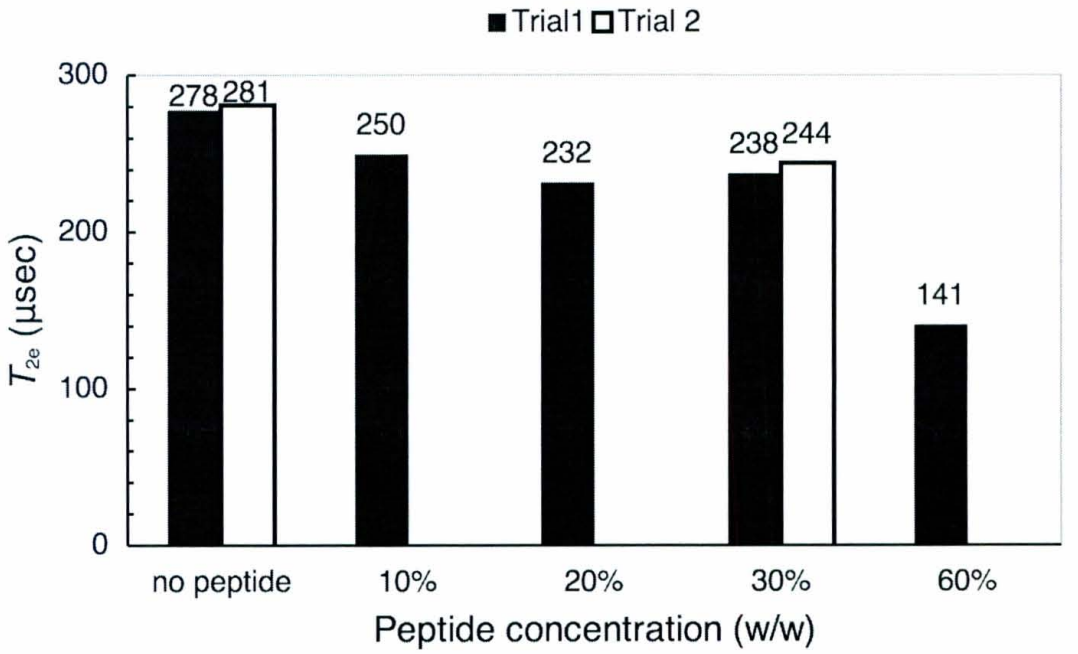

Figure 25. NMR quadrupolar echo decay time $|T_{2e}|$ at 37°C for membrane-deuterated LA8 bacteria, showing the effect of increasing concentrations of MSI-78.

4. Discussion

This study provides the first published NMR observations of AMP-induced lipid membrane disruption in whole bacteria. It is also the first to present NMR observations of whole bacteria with deuterium labeled unsaturated lipid chains, undergoing AMP-induced lipid membrane disruptions. During the course of this study, a novel strain of *E. coli* (LA8) was created and characterized for use in ^{2}H NMR studies of whole cells containing deuterated saturated chains.

Initial experiments began with the K1060 strain, which allowed incorporation of unsaturated labels (deuterated oleic acid) into the membrane for ^{2}H NMR studies. K1060 cells cultured in glucose produced narrow spectra characteristic of highly disordered chains along with a sharp central peak corresponding to deuterated water. It is possible that these spectra could reflect significant bacterial degradation given the intensity at the lower splittings, which corresponds to bacterial degradation as noted by Davis et al. [80]. However, because the signal-to-noise ratio is very poor in these spectra, it is difficult to draw definitive conclusions. The levels of deuterated water in the sample are quite significant, which is most likely a by-product of the transport of deuterated oleic acid into the cell. This transport involves the modification of the carboxyl group of the fatty acid, resulting in the transfer of the carboxyl deuterons to water [61].

In hopes of improving the spectra for the K1060 strain, cells were also cultured using casamino acids as the carbon source instead of glucose. K1060 cells cultured in casamino acids produced spectra with more prominent spectral edges than K1060 cells

cultured in glucose. This suggests cells cultured in glucose display more membrane disruption – likely associated with cell death – than cells cultured in casamino acids. A possible explanation could come from looking at how cells respond to stress conditions, such as those associated with preparing K1060 cells for ^{2}H NMR studies. When the K1060 cells are prepared for ^{2}H NMR studies, the various washing steps result in a depletion of nutrients. The only source of nutrients (carbon source) comes from dying cells; as they die, they release utilizable carbon into the media that can be used by neighboring cells. The major nutrient released by the dying cells might be amino acids, since proteins account for over 50% of the dry weight of *E. coli* [96]. Therefore, K1060 cells already adapted to casamino acids could more easily utilize the amino acids released by dying cells, thereby overcoming the nutrient deficiency. This could result in K1060 cells cultured in casamino acids dying off at a slower rate than those cultured in glucose. This is supported by work done by Zinser and Kolter (1999), who were looking at *E. coli* mutants that could survive during prolonged periods of starvations [97]. These mutants showed a preference for a mixture of amino acids (casamino acids) as their carbon source. Based on these results, media supplemented with casamino acids, rather than glucose, were used for all remaining K1060 experiments.

The next experiments looked at the effects of MSI-78 on the ^{2}H NMR spectra for K1060. Addition of MSI-78 led to a shift in intensity towards the center of the spectra. This suggests a decrease in the orientational order parameter resulting from increases in lipid disorder, which is an expected effect of MSI-78. However, the peptide was introduced into the sample via vortexing prior to ^{2}H NMR studies. Vortexing-based

techniques have been used in the past in order to disrupt bacterial cells [98]. It is likely that the observed effects on lipid disorder are due to vortexing rather than the effects of MSI-78. To confirm this possibility, control experiments looking at the effects of vortexing were conducted. These showed a similar shift in intensity towards the center of the spectra. This suggests that vortexing alone can significantly increase lipid disorder, with the effects possibly amplified in the presence of MSI-78. The shapes of the spectra for K1060 were quantified and expressed as M_1, M_2 and Δ_2. Vortexing led to lower values of M_1, confirming the increase in lipid disorder seen in the spectra. Addition of 10% MSI-78 led to only a slight increase in lipid disorder based on the calculated decrease in M_1. Addition of 20% MSI-78 was expected to lead to a further decrease in M_1 but instead the result was similar to the vortexed sample. This suggests that the peptide does not have much effect on lipid disorder and that the observed changes are predominantly due to vortexing. This might not be surprising, given that the unsaturated chain is already quite disordered to begin with [65]. As such, greater care was taken when preparing bacterial samples for later studies; peptide was introduced into the sample with gentle agitation.

In addition to the moment calculations, echo decay times were also calculated for the K1060 strain. Quadrupole echo decay reflects motions that change the orientation-dependent quadrupole interaction on a timescale comparable to the time over which the echo is formed. In the liquid crystalline phase, quadrupole echo decay can reflect slow motions like bilayer undulations, and faster motions like lipid wobble and reorientation about the bilayer normal [99]. For such faster motions, the

contribution to the echo decay rate is proportional to the second moment of that portion of the quadrupole interaction modulated by the motion; this is a parameter related to the amplitude of the motion. Liposomes made of 1-palmitoyl-2-oleoyl-sn-glycerol-3-phosphoethanolamine (POPE) mimicking bacterial membranes and deuterated at C-16 of oleic acid have a decay time of ≈1588 μs at 30°C [100]. Decay times observed for the K1060 strain were significantly lower than those observed for POPE liposomes, with a further decrease in the presence of MSI-78. Assuming that correlation times are not significantly increased, this might reflect a significant disordering of the unsaturated chain in the membranes of the K1060 strain.

Unfortunately, it is very difficult to interpret the results of ^{2}H NMR studies of the K1060 strain, since there are very few published papers with ^{2}H data on the unsaturated chain with which to compare my results. Additionally, the order parameter profile for deuterated oleic acid – the label on the K1060 strain – is not monotonically decreasing, i.e. the orientational order parameter does not steadily decrease as go down the chain (65). This makes it difficult to interpret the order parameter profile in order to compare it to the moment analysis of the K1060 strain. On the contrary, there has been considerable work done using deuterated saturated chains; as such it would be worthwhile to perform ^{2}H NMR studies of whole bacteria with the saturated chain labeled. In order to accomplish this, a novel strain of *E. coli* called LA8 was created (section 2.4). This strain is notable for having deuterated palmitic acid (saturated chain) incorporated into its membrane.

Initial ^{2}H NMR studies of LA8 with labeled saturated chains were done using the less sensitive 3.5 T spectrometer. This was the only spectrometer available at the time and as expected it produced spectra with poor signal-to-noise ratios. Because of the weak signal, tuning and phasing were likely sub-optimal for the LA8 experiments performed at 3.5 T. In hopes of improving the spectra for the LA8 cells, ^{2}H NMR studies were performed using a shorter recycling delay and a larger pulse separation than those used in earlier studies reported here. The acquisition parameters chosen were based on ones used by Davis et al. [80]. The larger pulse separation reduces signal intensity but also reduces the possibility of distortion due to preamplifier recovery. The shorter recycling delay allows for more scans over the same time period, increasing signal strength; however, it also shortens the time the deuterium nuclei have to equilibrate before each scan, possibly distorting the spectra. The ^{2}H NMR spectra acquired using the new pulse parameters appeared to have slightly better signal-to-noise ratios but it is very difficult to be sure.

In order to determine if the new pulse parameters produce significantly better spectra with LA8, ^{2}H NMR studies were done using a spectrometer with a more powerful magnet. The more powerful magnet increases the equilibrium net magnetization of the deuterium nuclei, significantly improving the signal-to-noise ratio. ^{2}H NMR spectra of LA8 acquired using the 9.4 T spectrometer (more powerful magnet) showed a significant improvement in the noise-to-noise ratio. Given the improvement seen using the 9.4 T spectrometer, ^{2}H NMR studies were conducted using earlier pulse parameters: a longer recycling delay and shorter pulse separation. These spectra not

only showed improved noise-to-noise ratios but also distinctive spectral edges. This is most likely associated with the increased intensity due to a shorter pulse separation and to allowing the deuterium nuclei to equilibrate with a longer recycling delay.

Shortening the processing time and isolating cells in the exponential phase of growth can also further improve the signal-to-noise ratio. The majority of new membrane synthesis takes place in the exponential phase of growth when most cells are dividing [38]. LA8 samples harvested in this phase will have the highest probability of deuterium labels being incorporated into the membrane exclusively, improving signal-to-noise ratio.

Once the ideal conditions for preparing the LA8 strain were determined, the biological effects of processing and prolonged periods of nutrient deficiency during the ^{2}H NMR study were addressed. This was done by measuring the cell viability through plate count and MTT assays. Surprisingly, the two assays did not agree with each other. The plate count assay showed a significant loss of viability due to processing and further decreases with prolonged periods of starvation. The MTT assay showed a moderate decrease in viability due to processing and was fairly constant during prolonged periods of starvation. This suggests that the processing and nutrient deficiencies – unavoidable consequences of ^{2}H NMR studies – resulted in the LA8 cells losing their ability to divide but remaining metabolically active. This phenomenon of being viable but nonculturable (VBNC) is not novel. Several bacteria including *E. coli* are able to switch to the VBNC state, usually in response to environmental stressors such as elevated osmotic concentrations, changes in pH, changes in temperature and nutrient deficiencies [101].

When bacterial cells are stressed, nucleic acid synthesis is inhibited and the bacterial genome becomes more compact due to supercoiling [102]. This might result in a shut down of the transcription of genes essential for cell division. Once these cells are placed in a nutrient-rich media – like that used in cell counts – the abundance of nutrients can be toxic to the cell, preventing colony development [101].

Since LA8 is a novel mutant of *E. coli*, it was necessary to determine the MIC value for the strain with respect to MSI-78. LA8 had an MIC value four times lower than for wild-type *E. coli*. This means that a significantly lower concentration of MSI-78 is needed in order to inhibit cell growth. Previous studies indicate the likely mechanism of action of MSI-78 involves membrane disintegration [71]. The lower peptide concentration requirement for LA8 suggests that the membrane might be more sensitive to MSI-78, i.e. the membranes of LA8 are already partially disintegrated or less robust than wild type *E. coli*.

The effects of MSI-78 were examined by conducting ^{2}H NMR studies of LA8 treated with different concentrations of MSI-78. Substantial and reproducible changes in the overall orientational order (M_1), the second moment (M_2) and the relative mean square width of the splitting distribution (Δ_2) derived from spectra of ^{2}H-membrane-labeled *E. coli* were observed with the addition of the AMP MSI-78. Decreases in orientational order parameter derive from increases in lipid disorder (increased angular amplitude of lipid chain motions) and thus M_1 directly reports on the lipid bilayer disruption proposed to be central to the function of AMPs. Changes in M_2 and Δ_2 provide additional characterization of how the spectral shape changes in response to

peptide-induced disruption. A key consideration with regards to the utility of ^{2}H measurements in whole bacteria is that solid-state NMR studies of AMPs in model lipid bilayers have been one of the cornerstones of the study of AMP mechanisms. Thus, comparing the results of NMR data in whole bacteria and model lipid systems should provide useful insights into the interpretation of AMP effects *in vivo*.

For such comparisons to be meaningful, it was important to first characterize the ^{2}H-membrane-labeled bacteria employed in the NMR studies. The LA8 bacteria used in this study were similar to the L51 strain used in studies of bacterial membranes in the 1970s [80] and the untreated bacteria gave rise to similar NMR spectra at 37 °C. The stability of the ^{2}H-NMR spectra of the ^{2}H-membrane-labeled LA8 cells was characterized over time. Slow changes in spectral moments was observed over the 18-hour experiment, which is not surprising, as the cells do not have access to nutrients during the NMR experiment. The spectral change over this period was small compared to the effect of treating with peptide and the rate of change was similar for all samples assayed - both treated and untreated. Likewise, duplicate experiments with fresh bacterial cell preparations confirmed these observations for both control and AMP-treated cells. Thus, it appears that the effects of the AMP treatments take place before the NMR experiments begin. The absence of any AMP-induced change in the M_1 versus time slope is consistent with the low levels of AMP used relative to the MIC, and allows us to compare the effect of the peptide on the spectra using an average of the first 8 hours of NMR data acquired.

To compare the NMR data from the ^{2}H-membrane-labeled cells to NMR data from model lipid systems or to cell growth AMP inhibition assays, it is useful to re-calculate the AMP amounts used in terms of molar peptide:lipid (P:L) ratios, in particular in terms of bacteria-bound P:L ratios. Typically, 10-95% of an AMP binds to the bacteria within 10-15 minutes [41], [103]. Since MSI-78 has an overall charge of +9, it would be expected to bind more tightly and quickly than an average AMP, and so is likely to be nearer the top of this 10-95% range. When calculated assuming 100% of MSI-78 is bacteria-bound, the w/w ratios of peptide:bacteria used in this study of 10%, 20%, 30%, and 60%, convert to molar bound P:L ratios of 0.31:1, 0.63:1, 0.94:1, and 1.9:1, respectively. This calculation uses my measurements of bacterial dry weight, and assumes lipids comprise 9.1% of the bacterial dry weight and have an average molecular weight of 705 g / mol [52].

Typical bound P:L ratios needed to inhibit bacterial growth in assays for AMP antimicrobial activity are 100:1 [41]. This is ≈100 times more peptide than was used in this study. However, for the LA8 strain the P:L ratio is four times less, possibly as a result of the membranes already being less robust or partially disintegrated. As such, it appears that the AMP-lipid interaction being observed in the current work is in the sublethal range. Hence, it can be concluded that some level of AMP-induced bilayer disruption does occur at levels well below those where cell growth inhibition takes place. This suggests some interesting possibilities regarding the two proposed classes of killing mechanism for AMPs in general. For AMPs that are thought to act primarily by membrane disruption, it raises the possibility that a notable amount of AMP-induced

membrane disruption can be tolerated before actual growth inhibition or cell death occurs. For AMPs that are thought to act on intracellular targets and whose interaction with the membrane is thus thought to be only that required to enter the cell, it suggests that even at relatively low levels of AMP there may be bilayer disruption and a consequent increased permeability to the AMP.

On the other hand, the P:L ratio required to see reductions in lipid chain order in the ^{2}H-membrane-labelled bacteria was much higher than those needed to see comparable changes in model lipid bilayers. Typical AMP:lipid ratios needed to see leakage in vesicle studies are 1:100 (total peptide) to 1:200 (bound peptide) [41]. In ^{2}H-NMR studies with model lipid membranes, AMP-induced decreases in lipid order are typically seen at concentrations of 1-3:100 or less (e.g. [99], [95]). For MSI-78, Ramamoorthy et al. showed dye leakage at P:L ratios as low as 1:1000 (in POPC/POPG) and observed a decrease in order parameter of ≈23% at a P:L ratio of 3:100 [71]. In the context of whole bacteria, the amount of peptide required to produce comparable changes in chain order is ~1:1, i.e. approximately 33 times more peptide than used in the Ramamoorthy et al. study.

There are at least two possible reasons why more peptide is needed to see comparable effects on the membrane of whole bacteria compared to model lipid bilayers. One possibility is that most of the peptide reaches the inner membrane but, for some reason, is less able to disrupt bilayer chain order at low concentrations than is the case in model systems where low concentrations are sufficient to cause observable effects. A more likely possibility, though, is that much of the peptide does not reach the

inner membrane. It may be bound up in other components of the Gram-negative cell envelope, such as the LPS layer. Substantial and disruptive interactions between LPS and MSI-78's parent peptide, magainin-2, have previously been observed [71, 104, 105]. More generally, the importance of non-phospholipid components of the bacterial cell wall has been suggested. Examples include the existence of some AMPs that appear to be able to act without crossing the outer membrane of Gram-negative bacteria (e.g. [73]) and observations that cell wall thickness correlates with AMP-resistance in methicillin-resistant *Staphylococcus aureus* (MRSA) [106].

In the future, the experimental framework employed in this study can be used with other peptides for a better understanding of AMP interactions with cell membranes. It would be interesting to see if AMPs with a similar antimicrobial activity as MSI-78 display a similar effect. By testing a variety of different AMPs new patterns might emerge better reflecting the understaning of AMP action *In vivo*.

In conclusion, this study has shows it is possible to obtain reproducible ^{2}H NMR spectra of membrane-deuterated bacteria in the absence and presence of the AMP MSI-78. The addition of MSI-78 leads to decreases in the order of the acyl chains in bacteria. The P:L ratios needed to observed MSI-78's effects on acyl chain order is intermediate between the ratios required to observe effects in biophysical studies of model lipid systems and the ratios required to observe inhibition of cell growth in biological assays.

References

1. Jenssen, H., Hamill, P., and Hancock, R. E. (2006) Peptide antimicrobial agents. Clin Microbiol Rev 19, 491-511.

2. Sato, H., and Feix, J. B. (2006) Peptide-membrane interactions and mechanisms of membrane destruction by amphipathic alpha-helical antimicrobial peptides. Biochim Biophys Acta 1758, 1245-1256.

3. Boucher, H. W., Talbot, G. H., Bradley, J. S., Edwards, J. E., Gilbert, D., Rice, L. B., Scheld, M., Spellberg, B., and Bartlett, J. (2009) Bad bugs, no drugs: no ESKAPE! An update from the Infectious Diseases Society of America. Clin Infect Dis 48, 1-12.

4. Falagas, M. E., and Bliziotis, I. A. (2007) Pandrug-resistant Gram-negative bacteria: the dawn of the post antibiotic era? Int J Antimicrob Agents 29, 630-636.

5. Falagas, M. E., and Kasiakou, S. K. (2005) Colistin: The Revival of Polymyxins for the Management of Multidrug-Resistant Gram-Negative Bacterial Infections. Clin Infect Dis 40, 1333-1341.

6. Chopra, I., Schofield, C., Everett, M., O'Neill, A., Miller, K., Wilcox, M., Frere, J., Dawson, M. J., Czaplewski, L., Urleb, U., and Courvalin, P. (2008) Treatment of health-care-associated infections caused by Gram-negative bacteria: a consensus statment. Lancet Infect Dis 8, 133-139.

7. Gordon, Y. J., and Romanowski, E. G. (2005) A Review of Antimicrobial Peptides and Their Therapeutic Potential as Anti-Infective Drugs. Curr Eye Res 30, 505-515.

8. Zasloff, M. (2002) Antimicrobial peptides of multicellular organisms. Nature 415, 389-395.

9. Brogden, K. A. (2005) Antimicrobial peptides: pore formers or metabolic inhibitors in bacteria? Nat Rev Microbiol 3, 238-250.

10. Aggarwal, K., and Silverman, N. (2008) Positive and negative regulation of the Drosophila immune response. BMB Rep 41, 267-277.

11. Giuliani, A., Pirri, G., and Nicoletto, S. F. (2007) Antimicrobial peptides: an overview of a promising class of therapeutics Central European Journal of Biology 2, 1-33.

12. Spitznagel, J. K. (1998) Origins and development of peptide antibiotic research: from extracts to abstracts to contracts. Mol Biotech 10, 237-245.

13. Skarnes, R. C., and Watson, D. W. (1957) Antimicrobial factors of normal tissues and fluids. Bacteriol Rev 4, 273-294.

14. Zasloff, M. (1987) Magainins, a class of antimicrobial peptides from Xenous skin: Isolation, characterization of two active forms, and partial cDNA sequence of precursor. Proc Natl Acad Sci U S A 84, 5449-5453.

15. Ganz, T., Selsted, M. E., and Lehrer, R. I. (1990) Defensins. Eur J Haematol 44, 1-8.

16. Steiner, H., Andreu, D., and Merrifield, R. B. (1988) Binding and action of cecropin and cecropin analogues: antibacterial peptides from insects. Biochim Biophys Acta 939, 260-266.

17. Hale, J. D., and Hancock, R. E. (2007) Alternative mechanisms of action of cationic antimicrobial peptides on bacteria. Expert Rev Anti Infect Ther 5, 951-959.

18. Cudic, M., and Otvos, L. J. (2002) Intracellular targets of antibacterial peptides. Curr Drug Targets 3, 101-106.

19. Tecle, T., Tripathi, S., and Hartshorn, K. L. (2010) Review: Defensins and cathelicidins in lung immunity. Innate Immun 16, 151-159.

20. Allaker, R. P. (2008) Host defence peptides - a bridge between the innate and adaptive immune responses. Trans R Soc Trop Med Hyg 102, 3-4.

21. Marcos, J. F., and Gandía, M. (2009) Antimicrobial peptides: to membranes and beyond. Expert Opinion on Drug Discovery 4, 659-671.

22. Bechinger, B. (2009) Rationalizing the membrane interactions of cationic amphipathic antimicrobial peptides by their molecular shape. Current Opinion in Colloid & Interface Science 14, 349-355.

23. Bechinger, B. (2011) Insights into the mechanisms of action of host defence peptides from biophysical and structural investigations. J Pept Sci 17, 306-314.

24. Bhattacharjya, S., and Ramamoorthy, A. (2009) Multifunctional host defense peptides: functional and mechanistic insights from NMR structures of potent antimicrobial peptides. FEBS J 276, 6465-6473.

25. Fernandez, D. I., Gehman, J. D., and Separovic, F. (2009) Membrane interactions of antimicrobial peptides from Australian frogs. Biochim Biophys Acta 1788, 1630-1638.

26. Aisenbrey, C., Bertani, P., and Bechinger, B. (2010) Solid-state NMR investigations of membrane-associated antimicrobial peptides. Methods Mol Biol 618, 209-233.

27. Wu, Y., Huang, H. W., and Olah, G. A. (1990) Method of oriented circular dichroism. Biophys J 57, 797-806.

28. Joanne, P., Galanth, C., Goasdoue, N., Nicolas, P., Sagan, S., Lavielle, S., Chassaing, G., El Amri, C., and Alves, I. D. (2009) Lipid reorganization induced by membrane-active peptides probed using differential scanning calorimetry. Biochim Biophys Acta 1788, 1772-1781.

29. Ladokhin, A. S., Selsted, M. E., and White, S. H. (1997) Sizing membrane pores in lipid vesicles by leakage of co-encapsulated markers: pore formation by melittin. Biophys J 72, 1762-1766.

30. Xiong, Y. Q., Mukhopadhyay, K., Yeaman, M. R., Adler-Moore, J., and Bayer, A. S. (2005) Functional interrelationships between cell membrane and cell wall in antimicrobial peptide-mediated killing of *Staphylococcus aureus*. Antimicrob Agents Chemother 49, 3114-3121.

31. Marrink, S. J., de Vries, A. H., and Tieleman, D. P. (2009) Lipids on the move: Simulations of membrane pores, domains, stalks and curves. Biochim Biophys Acta 1788, 149-168.

32. Freire, J. M., Domingues, M. M., Matos, J., Melo, M. N., Veiga, A. S., Santos, N. C., and Castanho, M. A. (2011) Using zeta-potential measurements to quantify peptide partition to lipid membranes. Eur Biophys J 40, 481-487.

33. Slavik, J. (1982) Anilinonaphthalene sulfonate as a probe of membrane composition and function. Biochim Biophys Acta 694, 1-25.

34. Fantner, G. E., Barbero, R. J., Gray, D. S., and Belcher, A. M. (2010) Kinetics of antimicrobial peptide activity measured on individual bacterial cells using high-speed atomic force microscopy. Nat Nanotechnol 5, 280-285.

35. Chen, F. Y., Lee, M. T., and Huang, H. W. (2003) Evidence for Membrane Thinning Effect as the Mechanism for Peptide-Induced Pore Formation. Biophys J 84, 3751-3758.

36. Hartmann, M., Berditsch, M., Hawecker, J., Ardakani, M. F., Gerthsen, D., and Ulrich, A. S. (2010) Damage of the bacterial cell envelope by antimicrobial peptides gramicidin S and PGLa as revealed by transmission and scanning electron microscopy. Antimicrob Agents Chemother 54, 3132-3142.

37. Matsuzaki, K. (2009) Control of cell selectivity of antimicrobial peptides. Biochim Biophys Acta 1788, 1687-1692.

38. Ruiz, N., Kahne, D., and Silhavy, T. J. (2006) Advances in understanding bacterial outer-membrane biogenesis. Nat Rev Microbiol 4, 57-66.

39. Hancock, R. E., and Bell, A. (1988) Antibiotic uptake into Gram-Negative Bacteria. Eur. J. Clin. Microbiol. Infect. Dis. 7, 713-720.

40. Shai, Y. (1999) Mechanism of the binding, insertion and destablization of phospholipid bilayer membranes by a-helical antimicrobial and cell non-selective membrane-lytic peptides. Biochim Biophys Acta 1462, 55-70.

41. Wimley, W. C. (2010) Describing the mechanism of antimicrobial peptide action with the interfacial activity model. ACS Chem Biol 5, 905-917.

42. Baumann, G., and Mueller, P. (1974) A molecular model of membrane excitability. J Supramol Struct 2, 538-557.

43. Yang, L., Harroun, T. A., Weiss, T. M., Ding, L., and Huang, H. W. (2001) Barrel-Stave Model or Toroidal Model? A case study on Melittin Pores. Biophys J 81, 1475-1485.

44. Bocchinfuso, G., Palleschi, A., Orioni, B., Grande, G., Formaggio, F., Toniolo, C., Park, Y., Hahm, K. S., and Stella, L. (2009) Different mechanisms of action of antimicrobial peptides: insights from fluorescence spectroscopy experiments and molecular dynamics simulations. J Pept Sci 15, 550-558.

45. Ludtke, S. J., He, K., Heller, W. T., Harroun, T. A., Yang, L., and Huang, H. W. (1996) Membrane pores induced by magainin. Biochemistry 35, 13723-13728.

46. Uzarski, J. R., Tannous, A., Morris, J. R., and Mello, C. M. (2008) The effects of solution structure on the surface conformation and orientation of a cysteine-terminated antimicrobial peptide cecropin P1. Colloids Surf B Biointerfaces 67, 157-165.

47. Epand, R. M., and Epand, R. F. (2009) Lipid domains in bacterial membranes and the action of antimicrobial agents. Biochim Biophys Acta 1788, 289-294.

48. Dosanjh, N. S., and Michel, S. L. (2006) Microbial nickel metalloregulation: NikRs for nickel ions. Curr Opin Chem Biol 10, 123-130.

49. Sutcliffe, I. C. (2010) A phylum level perspective on bacterial cell envelope architecture. Trends Microbiol 18, 464-470.

50. Itoh, S. (2006) Mononuclear copper active-oxygen complexes. Current Opinion in Chemical Biology 10, 115-122.

51. Cronan, J. E. (2006) A bacterium that has three pathways to regulate membrane lipid fluidity. Mol Microbiol 60, 256-259.

52. Neidhardt, F. C., and Curtiss, R. (1996) *Escherichia coli* and Salmonella: Cellular and molecular biology 1, 14.

53. Melo, M. N., Ferre, R., and Castanho, M. A. R. B. (2009) Antimicrobial peptides: linking partition, activity and high membrane-bound concentrations. Nat Rev Microbiol 7, 245-250.

54. Piers, K. L., and Hancock, R. E. W. (1994) The interaction of a recombinant cecropin/melittin hybrid peptide with the outer membrane of *Pseudomonas aeruginosa*. Mol Microbiol 12, 951-958.

55. Ramamoorthy, A., Thennarasu, S., Tan, A., Lee, D. K., Clayberger, C., and Krensky, A. M. (2006) Cell selectivity correlates with membrane-specific interactions: A case study on the antimicrobial peptide G15 derived from granulysin. Biochim Biophys Acta 1758, 154-163.

56. White, S. W., Zheng, J., Zhang, Y. M., and Rock, C. O. (2005) The structural biology of type II fatty acid biosynthesis. Annu Rev Biochem 74, 791-831.

57. Cronan Jr, J. E., and Waldrop, G. L. (2002) Multi-subunit acetyl-CoA carboxylases. Progress in Lipid Research 41, 407-435.

58. Zhang, Y. M., and Rock, C. O. (2008) Membrane lipid homeostasis in bacteria. Nat Rev Microbiol 6, 222-233.

59. Lu, Y. J., Zhang, Y. M., Grimes, K. D., Qi, J., Lee, R. E., and Rock, C. O. (2006) Acyl-phosphates initiate membrane phospholipid synthesis in Gram-positive pathogens. Mol Cell 1, 765-772.

60. Brigham, C. J., Budde, C. F., Holder, J. W., Zeng, Q., Mahan, A. E., Rha, C., and Sinskey, A. J. (2010) Elucidation of beta-oxidation pathways in *Ralstonia eutropha* H16 by examination of global gene expression. J Bacteriol 192, 5454-5464.

61. Campbell, J. W., and Cronan Jr, J. E. (2002) The enigmatic Escherichia coli fadE gene is yafH. Journal of Bacteriology 184, 3759.

62. Overath, P., Schairer, H. U., and Stoffel, W. (1970) Correlation of In Vivo and In Vitro Phase Transitions of Membrane Lipids in *Escherichia coli*. Proc Natl Acad Sci U S A 67, 606-612.

63. Harder, M. E., Beacham, I. R., Cronan Jr, J. E., Beacham, K., Honegger, J. L., and Silbert, D. F. (1972) Temperature-Sensitive Mutants of Escherichia coli Requiring Saturated and Unsaturated Fatty Acids for Growth: Isolation and Properties. Proc Natl Acad Sci USA 69, 3105-3109.

64. Konings, A. W. T., Gipp, J. J., and Yatvin, M. B. (1984) Radio- and Thermosenstivity of E. coli K1060 after Thiol Depletion by Diethylmaleate. Radiation and Environmental Biophysics 23, 245-253.

65. Seelig, J., and Waespe-Sarcevic, N. (1978) Molecular Order in Cis and Trans Unsaturated Phospholipid Bilayers. Biochemistry 17, 3310-3315.

66. Nichol, C. P., Davis, J. H., Weeks, G., and Bloom, M. (1980) Quantitative Study of the Fluidity of Escherichia coli Membranes Using Deuterium Magnetic Resonance. Biochemistry 19, 451-457.

67. Bloom, M., and Sternin, E. (1987) Transverse nuclear spin relaxation in phospholipid bilayer membranes. Biochemistry 26, 2101-2105.

68. Kwak, S., Brief, E., Langlais, D., Kitson, N., Lafleur, M., and Thewalt, J. (2012) Ethanol perturbs lipid organization in models of stratum corneum membranes: An investigation combining differential scanning calorimetry, infrared and (2)H NMR spectroscopy. Biochim Biophys Acta 1818 (5), 1410-1419.

69. Silbert, D. F., Pohlman, R., and Chapman, A. (1976) Partial Characterization of a Temperature-Sensitive Mutation Affecting Acetyl Coenzyme A Carboxylase in Escherichia coli K-12. Journal of Bacteriology 126, 1351-1354.

70. Hallock, K. J., Lee, D. K., and Ramamoorthy, A. (2003) MSI-78, an analogue of the magainin antimicrobial peptides, disrupts lipid bilayer structure via positive curvature strain. Biophys J 84, 3052-3060.

71. Ramamoorthy, A., Thennarasu, S., Lee, D. K., Tan, A., and Maloy, L. (2006) Solid-state NMR investigation of the membrane-disrupting mechanism of antimicrobial peptides MSI-78 and MSI-594 derived from magainin 2 and melittin. Biophys J 91, 206-216.

72. Porcelli, F., Buck-Koehntop, B. A., Thennarasu, S., Ramamoorthy, A., and Veglia, G. (2006) Structures of the dimeric and monomeric variants of magainin antimicrobial

peptides (MSI-78 and MSI-594) in micelles and bilayers, determined by NMR spectroscopy. Biochemistry 45, 5793-5799.

73. Epand, R. F., Sarig, H., Mor, A., and Epand, R. M. (2009) Cell-wall interactions and the selective bacteriostatic activity of a miniature oligo-acyl-lysyl. Biophys J 97, 2250-2257.

74. Roth, M. R., and Welti, R. (1994) Arrangement of phosphatidylethanolamine molecular species in Escherichia coli membranes and reconstituted lipids as determined by dimethyl suberimidate cross-linking of nearest neighbor lipids. Biochim Biophys Acta 1190, 91-98.

75. Datsenko, K. A., and Wanner, B. L. (2000) One-step inactivation of chromosonal genes in *Escherchia coli* K-12 using PCR products. Proc Natl Acad Sci U S A 97, 6640-6645.

76. Yamamoto, S., Izumiya, H., Morita, M., Arakawa, E., and Watanabe, H. (2009) Application of lambda Red recombination system to *Vibrio cholerae* genetics: simple methods for inactivation and modification of chromosomal genes. Gene 438, 57-64.

77. Davis, J. H., Jeffrey, K. R., Bloom, M., Valic, M. I., and Higgs, T. P. (1976) Quadrupolar echo deuteron magnetic resonance spectroscopy in ordered hydrocarbon chains. Chemical Physics Letters 42, 390-394.

78. Prosser, R. S., Davis, J. H., Dahlquist, F. W., and Lindorfer, M. A. (1991) Deuterium nuclear magnetic resonance of the gramicidin A backbone in phospholipid bilayer. Biochemistry 30, 4687-4696.

79. Bonev, B., and Morrow, M. R. (1996) Effects of Hydrostatic Pressure on Bilayer Phase Behavior and Dynamics of Dilauroylphosphatidylcholine. Biophys J 70, 2727-2735.

80. Davis, J. H., Nichol, C. P., Weeks, G., and Bloom, M. (1979) Study of the Cytoplasmic and Outer Membranes of *Escherichia Coli* by Deuterium Magnetic Resonance. Biochemistry 18, 2103 - 2112.

81. Davis, J. H. (1983) The description of membrane lipid conformation, order and dynamics by 2H-NMR. Biochim Biophys Acta 737, 117-171.

82. Wang, H., Cheng, H., Wang, F., Wei, D., and Wang, X. (2010) An improved 3-(4,5-dimethylthiazol-2-yl)-2,5-diphenyl tetrazolium bromide (MTT) reduction assay for evaluating the viability of *Escherichia coli* cells. J Microbiol Methods 82, 330-333.

83. Wiegand, I., Hilpert, K., and Hancock, R. E. (2008) Agar and broth dilution methods to determine the minimal inhibitory concentration (MIC) of antimicrobial substances. Nature Protocols 3, 163-175.

84. Gally, H. U., Pluschke, G., Overath, P., and Seelig, J. (1979) Structure of *Escherichia coli* membranes. Phospholipid conformation in model membranes and cells as studied by deuterium magnetic resonance. Biochemistry 18, 5605-5610.

85. Olsen, W. L., Schaechter, M., and Khorana, H. G. (1979) Incorporation of Synthetic Fatty Acid Analogs into Phospholipids of *Escherichia coli*. Journal of Bacteriology 137, 1443-1446.

86. Seelig, J. (2009) Deuterium magnetic resonance: theory and application to lipid membranes Quaterly Reviews of Biophysics 10 (3), 353-418.

87. Huang, T., DeSiervo, A. J., and Yang, Q. (1991) Effect of cholesterol and lanosterol on the structure and dynamics of the cell membrane of Mycoplasma capricolum. Biophys J 59, 691-702.

88. Silbert, D. F., Ulbright, T. M., and Honegger, J. L. (1973) Utilization of exogenous fatty acids for complex lipid biosynthesis and its effect on de novo fatty acid formation in *Escherichia coli* K-12. Biochemistry 12, 164-171.

89. Shaikh, S. R., Dumaual, A. C., Castillo, A., LoCascio, D., Siddiqui, R. A., Stillwell, W., and Wassall, S. R. (2004) Oleic and docosahexaenoic acid differentially phase separate from lipid raft molecules: a comparative NMR, DSC, AFM, and detergent extraction study. Biophys J 87, 1752-1766.

90. Cronan Jr, J. E. (1968) Phospholipid Alterations During Gorwth of *Escherichia coli*. Journal of Bacteriology 95, 2054-2061.

91. Russell-Schulz, B., Booth, V., and Morrow, M. R. (2009) Perturbation of DPPC/POPG bilayers by the N-terminal helix of lung surfactant protein SP-B: a (2)H NMR study. Eur Biophys J 38, 613-624.

92. Lafleur, M., Fine, B., Sternin, E., PR, C., and Myer, B. (1989) Smoothed orientational order profile of lipid bilayers by 2H-nuclear magnetic resonance. Biophys J 56, 1037-1041.

93. Davis, J. H. (1979) Deuterium Magnetic Resonance Study of the Gel and Liquid Crystalline Phases of Diplamitoyl Phosphatidylcholine. Biophys J 27, 339-358.

94. Morrow, M. R., Whitehead, J. P., and Lu, D. (1992) Chain-length dependence of lipid bilayer properties near the liquid crystal to gel phase transition. Biophys J 63, 18-27.

95. Fernandez, D. I., Sani, M. A., Gehman, J. D., Hahm, K. S., and Separovic, F. (2011) Interactions of a synthetic Leu-Lys-rich antimicrobial peptide with phospholipid bilayers. Eur Biophys J 40, 471-480.

96. Neidhardt, F. C., Ingraham, J. L., Low, K. B., Magasanik, B., Schaechter, M., and Umbarger, H. E. (1987) "Escherichia coli and Salmonella Typhimurium". American Society for Microbiology, Washington, DC.

97. Zinser, E. R., and Kolter, R. (1999) Mutations Enhancing Amino Acid Catabolism Confer a Growth Advantage in Stationary Phase. J. Bacteriol 181, 5800-5807.

98. Ranhand, J. M. (1974) Simple, Inexpensive Procedure for the Disruption of Bacteria. Appl Microbiol Biotechnol 28, 66-69.

99. Henzler-Wildman, K. A., Martinez, G. V., Brown, M. F., and Ramamoorthy, A. (2004) Perturbation of the hydrophobic core of lipid bilayers by the human antimicrobial peptide LL-37. Biochemistry 43, 8459-8469.

100. Smith, I. C. P., and Jarell, H. C. (1985) Acyl Chain Dynamics of Phosphatidylethanolamines Containing Oleic Acid and Dihyrdosterculic Acid: 2H NMR relaxation studies. Biochemistry 24, 4659-4665.

101. Oliver, J. D. (2005) The viable but nonculturable state in bacteria. The Journal of Microbiology 43, 93-100.

102. Warner, J. M., and Oliver, J. D. (1998) Randomly Amplified Polymorphic DNA Analysisof Starved and Viable but Nonculturable *Vibrio vulnificus* Cells. Appl Environ Microbiol 64, 3025-3028.

103. Tran, D., Tran, P. A., Tang, Y. Q., Yuan, J., Cole, T., and Selsted, M. E. (2002) Homodimeric theta-defensins from rhesus macaque leukocytes: isolation, synthesis, antimicrobial activities, and bacterial binding properties of the cyclic peptides. J Biol Chem 277, 3079-3084.

104. Matsuzaki, K., Sugishita, K., Harada, M., Fujii, N., and Miyajima, K. (1997) Interactions of an antimicrobial peptide, magainin 2, with outer and inner membranes of Gram-negative bacteria. Biochim Biophys Acta 1327, 119-130.

105. Matsuzaki, K., Sugishita, K., and Miyajima, K. (1999) Interactions of an antimicrobial peptide, magainin 2, with lipopolysaccharide-containing liposomes

as a model for outer membranes of Gram-negative bacteria. FEBS Lett 449, 221-224.

106. Mishra, N. N., McKinnell, J., Yeaman, M. R., Rubio, A., Nast, C. C., Chen, L., Kreiswirth, B. N., and Bayer, A. S. (2011) In vitro cross-resistance to daptomycin and host defense cationic antimicrobial peptides in clinical methicillin-resistant *Staphylococcus aureus* isolates. Antimicrob Agents Chemother 55, 4012-4018.

107. Baldassare, J.J., Rhinehart, K.B., and Silbert, D.R. (1976) Modification of membrane lipids: Physical properties in relation to fatty acid structure. Biochemistry 55, 2986-2994.

108. Han, X., Bushweller, J.H., Cafiso, D.S., and Tamm, L.K. (2001) Membrane structure and fusion-triggering conformational change of the fusion doman from influenza hemagglutinin. Nature Structural Biology 8, 715-720.

109. Reid, D.G. (1997) Protein NMR Techniques. Methods in Molecular Biology. Humana Press, Totowa, New Jersey. 419

Appendix

A.1 ^2H NMR studies of LA8 in a low field spectrometer

Using the LA8 strain, different options for NMR data acquisition were explored, which included modifying the pulse parameters used. Davis et al., [80] studied the effects of temperature on the cytoplasmic and outer membranes of *E. coli* by ^2H NMR, using a strain metabolically similar to LA8. However, they used a shorter recycling delay (i.e. more scans per second) and a longer pulse separation. In order to check for sensitivity of the observed signal to acquisition parameters, similar settings as those used by Davis et al. were tested when working with the LA8 strain. These initial tests with the LA8 strain were done at a lower field because of the availability of that spectrometer.

Initial experiments on the LA8 strain in the low field spectrometer were done using the pulse parameters defined in section 2.6. The low field spectrometer uses a less powerful magnet. As such, a lower signal-to-noise ratio is expected than compared to earlier ^2H NMR experiments. Since sensitivity is proportional to the $B_o^{3/2}$ (magnetic field), the expected decrease in sensitivity when going from 9.4T to 3.5T would be 77% [109].

^2H NMR spectra were recorded for LA8 cells cultured in Medium 63-B and harvested in the stationary phase. Appendix Figure 1 shows a series of spectra acquired at 37°C every 10 h, such that the first scan starts ≈2.5 h after the initial harvesting of bacteria. As expected, these spectra show poor signal to noise ratio. These spectra did not show spectral edges at ±15 kHz. Such edges, which are characteristic of

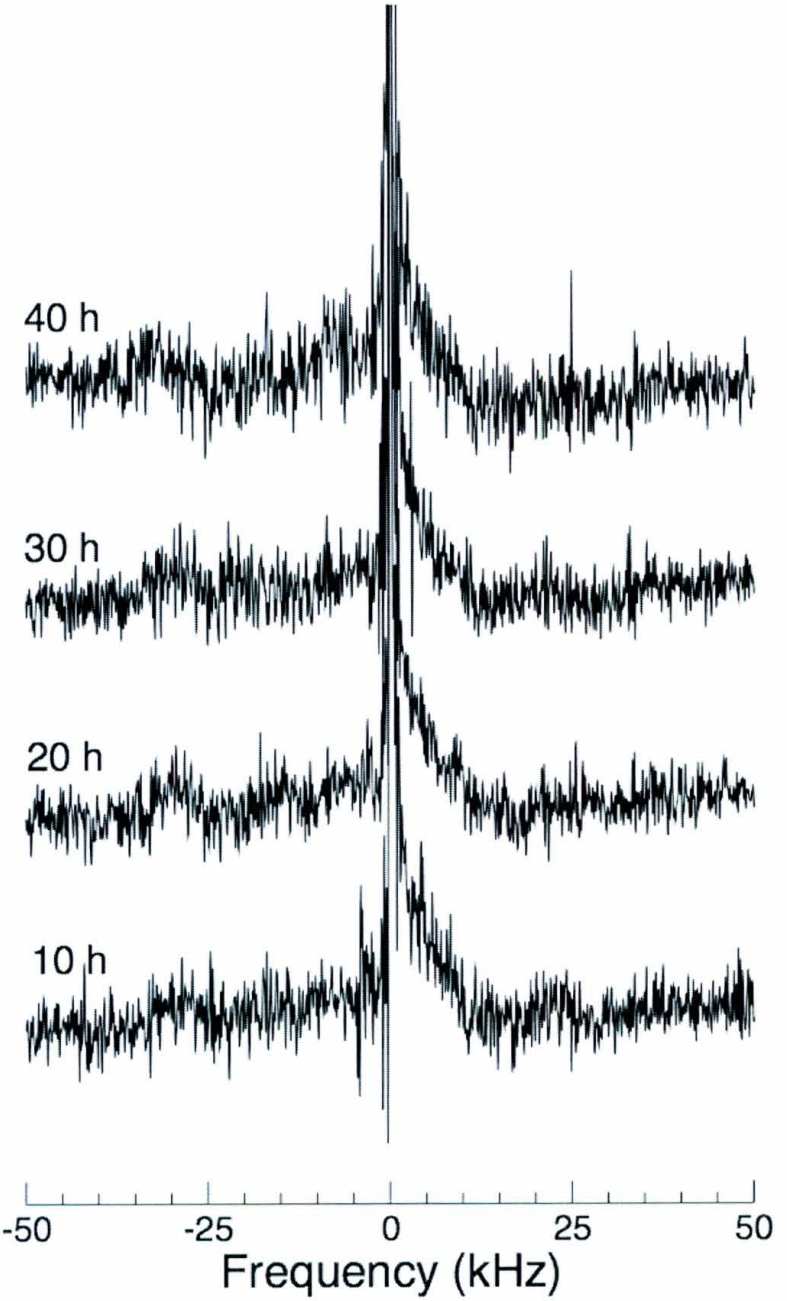

Appendix Figure 1. Solid-state 2H NMR spectra of membrane-deuterated LA8 bacteria, showing the evolution of the NMR spectra over time. Experiments were performed at 37°C using a 3.5 Tesla solid-state NMR spectrometer with a 900 ms recycling delay and 30 μs pulse separation. Each spectrum represents 40000 scans.

perdeuterated chains undergoing axially symmetric reorientation, are seen in the spectra of multilamellar vesicles of POPE prepared with deuterated palmitic acid (16:0-18:1PE-d_{31}) in the liquid crystalline phase [89]. The spectra observed here display increased intensity at the lower splittings relative to the higher splittings and are quite asymmetric, which likely reflects difficulties with optimal phasing of such weak signals. They also have a sharp, central peak with a width of <1 kHz, which arises because of naturally occurring deuterated water [71]. As time progresses, there are no visible changes in the spectra, which might suggest few changes to the lipid acyl chain order.

In order to check for sensitivity of the spectra to acquisition conditions, spectra were also collected using pulse parameters similar to those previously used by Davis et al. [80] (500 ms recycling delay and 40 μs pulse separation). Appendix Figure 2 shows a series of spectra acquired using the new pulse parameters. The spectra were collected at 37°C on the same 3.5 T spectrometer every 5 h, such that the first scan started ≈2.5 h after the initial harvesting of bacteria. The acquired spectra were very similar to the previous spectra (Appendix Figure 1); both sets have poor signal-to-noise ratio, a sharp central peak corresponding to deuterated water and no obvious spectral edges. One difference observed using the new pulse parameters was that the spectra were more symmetric, suggesting a better ability to optimize tuning and phasing.

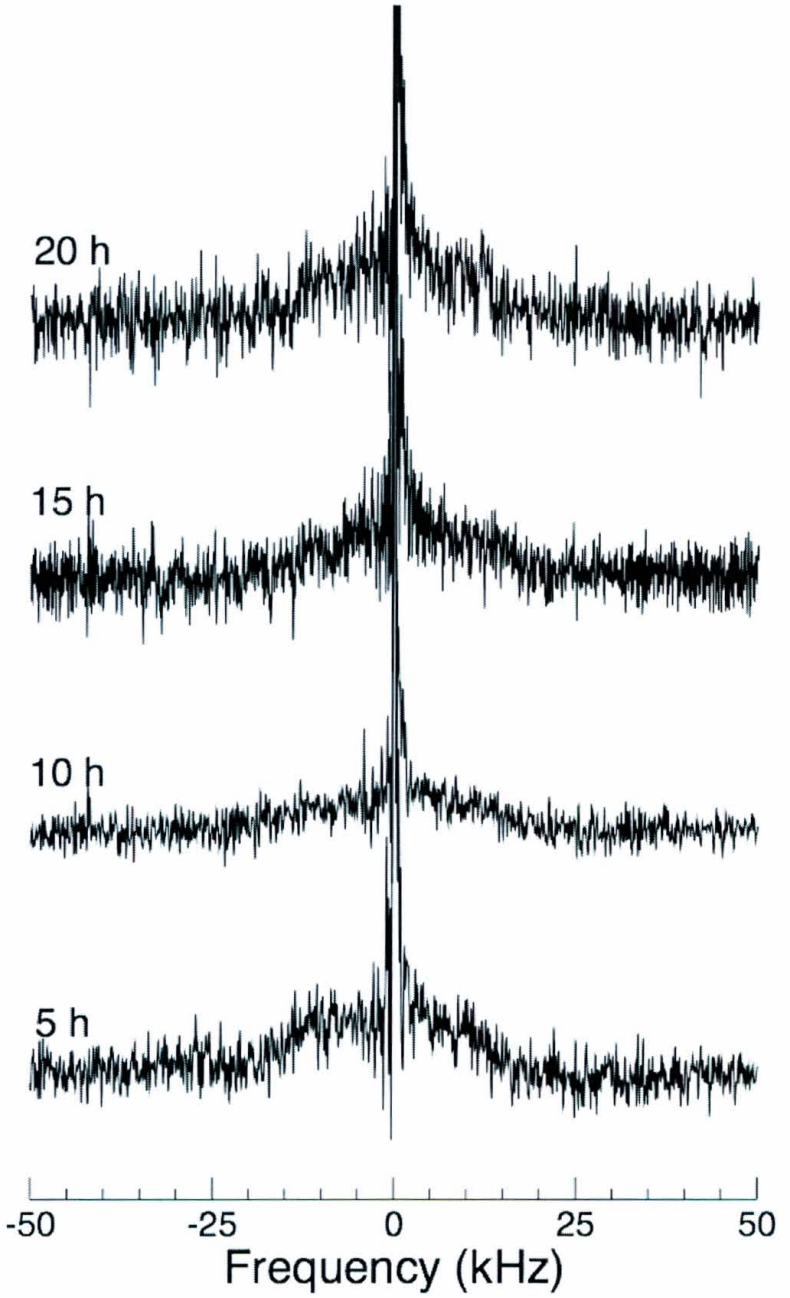

Appendix Figure 2. Solid-state ^{2}H NMR spectra of membrane-deuterated LA8 bacteria, showing the evolution of the NMR spectra over time. Experiments were performed at 37°C using a 3.5 Tesla solid-state NMR spectrometer with a 500 ms recycling delay and 40 μs pulse separation. Each spectrum represents 40000 scans.